Inorganic Chemistry

Article

pubs.acs.org/IC

Syntheses, Structures, and Magnetic Properties of Acetato- and Diphenolato-Bridged 3d−4f Binuclear Complexes [M(3-MeOsaltn)(MeOH)$_x$(ac)Ln(hfac)$_2$] (M = Zn^{II}, Cu^{II}, Ni^{II}, Co^{II}; Ln = La^{III}, Gd^{III}, Tb^{III}, Dy^{III}; 3-MeOsaltn = *N,N′*-Bis(3-methoxy-2-oxybenzylidene)-1,3-propanediaminato; ac = Acetato; hfac = Hexafluoroacetylacetonato; *x* = 0 or 1)

Masaaki Towatari,[†] Koshiro Nishi,[†] Takeshi Fujinami,[†] Naohide Matsumoto,*[,†] Yukinari Sunatsuki,[‡] Masaaki Kojima,[‡] Naotaka Mochida,[§] Takayuki Ishida,[§] Nazzareno Re,[∥] and Jerzy Mrozinski[⊥]

[†]Department of Chemistry, Faculty of Science, Kumamoto University, Kumamoto 860-8555, Japan

[‡]Department of Chemistry, Faculty of Science, Okayama University, Tsushima-naka 3-1-1, Okayama 700-8530, Japan

[§]Department of Engineering Science, The University of Electro-Communications, Chofu, Tokyo 182-8585, Japan

[∥]Facolta di Farmacià, Universita degli Studi "G.D 'Annunzio", I-66100 Chieti, Italy

[⊥]Faculty of Chemistry, University of Wroclaw, 14, F. Joliot-Curie, 50-383 Wroclaw, Poland

Supporting Information

ABSTRACT: A series of 3d−4f binuclear complexes, [M(3-MeOsaltn)(MeOH)$_x$(ac)Ln(hfac)$_2$] (*x* = 0 for M = Cu^{II}, Zn^{II}; *x* = 1 for M = Co^{II}, Ni^{II}; Ln = Gd^{III}, Tb^{III}, Dy^{III}, La^{III}), have been synthesized and characterized, where 3-MeOsaltn, ac, and hfac denote *N,N′*-bis(3-methoxy-2-oxybenzylidene)-1,3-propanediaminato, acetato, and hexafluoroacetylacetonato, respectively. The X-ray analyses demonstrated that all the complexes have an acetato- and diphenolato-bridged M^{II}−Ln^{III} binuclear structure. The Cu^{II}−Ln^{III} and Zn^{II}−Ln^{III} complexes are crystallized in an isomorphous triclinic space group $P\bar{1}$, where the Cu^{II} or Zn^{II} ion has square pyramidal coordination geometry with N_2O_2 donor atoms of 3-MeOsaltn at the equatorial coordination sites and one oxygen atom of the bridging acetato ion at the axial site. The Co^{II}−Ln^{III} and Ni^{II}−Ln^{III} complexes are crystallized in an isomorphous monoclinic space group $P2_1/c$, where the Co^{II} or Ni^{II} ion at the high-spin state has an octahedral coordination environment with N_2O_2 donor atoms of 3-MeOsaltn at the equatorial sites, and one oxygen atom of the bridged acetato and a methanol oxygen atom at the two axial sites. Each Ln^{III} ion for all the complexes is coordinated by four oxygen atoms of two phenolato and two methoxy oxygen atoms of "ligand-complex" M(3-MeOsaltn), four oxygen atoms of two hfac$^-$, and one oxygen atom of the bridging acetato ion; thus, the coordination number is nine. The temperature dependent magnetic susceptibilities from 1.9 to 300 K and the field-dependent magnetization up to 5 T at 1.9 K were measured. Due to the important orbital contributions of the Ln^{III} (Tb^{III}, Dy^{III}) and to a lesser extent the M^{II} (Ni^{II}, Co^{II}) components, the magnetic interaction between M^{II} and Ln^{III} ions were investigated by an empirical approach based on a comparison of the magnetic properties of the M^{II}−Ln^{III}, Zn^{II}−Ln^{III}, and M^{II}−La^{III} complexes. The differences of $\chi_M T$ and $M(H)$ values for the M^{II}−Ln^{III}, Zn^{II}−Ln^{III} and those for the M^{II}−La^{III} complexes, that is, $\Delta(T) = (\chi_M T)_{MLn} - (\chi_M T)_{ZnLn} - (\chi_M T)_{MLa} = J_{MLn}(T)$ and $\Delta(H) = M_{MLn}(H) - M_{ZnLn}(H) - M_{MLa}(H) = J_{MLn}(H)$, give the information of 3d−4f magnetic interaction. The magnetic interactions are ferromagnetic if M^{II} = (Cu^{II}, Ni^{II}, and Co^{II}) and Ln = (Gd^{III}, Tb^{III}, and Dy^{III}). The magnitudes of the ferromagnetic interaction, $J_{MLn}(T)$ and $J_{MLn}(H)$, are in the order Cu^{II}−Gd^{III} > Cu^{II}−Dy^{III} > Cu^{II}−Tb^{III}, while those are in the order of M^{II}−Gd^{III} ≈ M^{II}−Tb^{III} > M^{II}−Dy^{III} for M^{II} = Ni^{II} and Co^{II}. Alternating current (ac) susceptibility measurements demonstrated that the Ni^{II}−Tb^{III} and Co^{II}−Tb^{III} complexes showed out-of-phase signal with frequency-dependence and the Ni^{II}−Dy^{III} and Co^{II}−Dy^{III} complexes showed small frequency-dependence. The energy barrier for the spin flipping was estimated from the Arrhenius plot to be 14.9(6) and 17.0(4) K for the Ni^{II}−Tb^{III} and Co^{II}−Tb^{III} complexes, respectively, under a dc bias field of 1000 Oe.

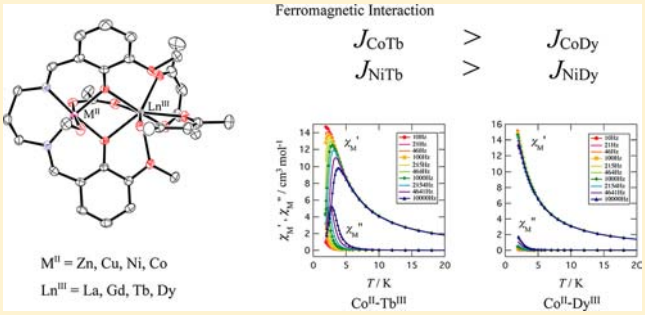

Received: March 10, 2013
Published: May 6, 2013

INTRODUCTION

The discovery of single molecule magnets (SMMs) in Mn_{12} cluster and the subsequent extensive developments are considered as one of the most important achievements of molecular magnetism.[1] The origin of the SMM behavior is the easy axis magnetic anisotropy ($D < 0$), which causes the formation of an energy barrier that prevents reversal of the molecular magnetization and causes a slow relaxation of the magnetization. SMMs can be formed as a result of the combination of a large-spin multiplicity of the ground state and an easy-axis (or Ising-type) magnetic anisotropy of the entire molecule. Although the conditions to be SMMs are not easily achieved by d-transition metal complexes, utilization of 4f ions, such as Tb^{III} and Dy^{III}, satisfies these conditions much more easily, because they have large angular momentum in the ground multiplet state and a large Ising-type magnetic anisotropy. Ishikawa et al. reported that Tb^{III}, Dy^{III}, and Ho^{III} phthalocyanines exhibit SMM behavior, and a molecule with only one Tb^{III} ion can indeed behave as SMM.[2] The d−f polynuclear structure gives a more suitable molecular design for SMMs, because the high-spin state is often generated by d−f magnetic interaction and the magnetic anisotropy can be derived from both f- and d-elements. Therefore, in recent years, molecular designs of SMMs and single chain magnets (SCMs) containing f-block elements have attracted much attention, although it should be noted that d−f complexes have been studied since the pioneering works of Gatteschi et al. on Cu^{II}−Gd^{III} complexes.[3] Matsumoto et al. reported the first 3d−4f cluster exhibiting frequency dependent out-of-phase ac signals, $[Cu^{II}LTb^{III}(hfac)_2]_2$ (H_3L = 1-(2-hydroxybenzamido)-2-(2-hydroxy-3-methoxy-benzylideneamino)-ethylene, and Hhfac = hexafluoroacetylacetone).[4] Christou's group[5] and Pecoraro's group[6] synthesized Mn^{III}−Dy^{III} clusters and reported their magnetic properties. $[Mn^{III}{}_{11}Dy^{III}{}_4]$ and $[Mn^{III}{}_2Dy^{III}{}_2]$ clusters reported by Christou's group[5] are confirmed to exhibit temperature and sweep rate dependent hysteresis loops, a trademark of all SMMs. Furthermore, many reports on d−f clusters, $[Cu^{II}Tb^{III}]$ binuclear, and $[Cu^{II}{}_2Tb^{III}{}_2]$ tetranuclear complexes,[7] $[Cu^{II}{}_4Tb^{III}]$ pentanuclear complex,[8] $[Cu^{II}{}_6Dy^{III}{}_3]$ nonanuclear complexes,[9] $[Fe^{III}Dy^{III}]$ binuclear complex,[10] and $[Ni^{II}Ln^{III}]$ binuclear complex containing paramagnetic Ni^{II} ion,[11] and $[Dy^{III}{}_6Mn^{III}{}_{12}]$ cores[12] have appeared in the latest literature. Kajiwara et al. reported two Cu^{II}−Tb^{III} binuclear complexes, in which the symmetry of the ligand field around the lanthanide ion strongly affects the magnetic anisotropy to induce a drastic switching from easy axis to easy-plane anisotropy, and one complex showed SMM behavior while the other one did not.[13] An approach within the framework of d−f clusters has been extended in the recent years. Chandrasekhar et al.[14a] reported a linear trinuclear Co^{II}−Gd^{III}−Co^{II} SMM, and Costes et al.[14b,c] reported trinuclear and tetranuclear Co^{II}−Gd^{III} SMMs, where Gd^{III} ion with an isotropic magnetic center and Co^{II} ion with highly anisotropic magnetic center are used. Many other d−f complexes of different nuclearities have been reported.[15] All these studies demonstrate that the d−f cluster approach is a promising pathway to SMMs, and that SMM behavior can be driven from many combinations of d- and f-metal ions.

In this study, in order to look for the possible combinations of d- and f-metal ions giving SMM behavior, according to the reaction procedure shown in Scheme 1, we synthesized the series of acetato- and diphenolato-bridged 3d−4f binuclear complexes, $[M(3\text{-MeOsaltn})(MeOH)_x(ac)Ln(hfac)_2]$ (x = 0 for M = Cu^{II}, Zn^{II}; x = 1 for M = Co^{II}, Ni^{II}; Ln = Gd^{III}, Tb^{III}, Dy^{III}, La^{III}), where 3-MeOsaltn, ac, and hfac denote *N*,*N*′-bis(3-methoxy-2-oxybenzylidene)-1,3-propanediaminato), acetate, and hexafluoroacetylacetonato, respectively.[16] Due to the suitable properties of tetradentate 3-MeOsaltn ligand, the Ni^{II} and Co^{II} ions assume high-spin states which are best suited to give SMMs when assembled with Ln^{III} species. A series of d−f binuclear complexes $[M(3\text{-MeOsaltn})(MeOH)_x(ac)Ln(hfac)_2]$ (M = Cu^{II}, Zn^{II}, Co^{II}, Ni^{II}; Ln = Gd^{III}, Tb^{III}, Dy^{III}, La^{III}) including diamagnetic Zn^{II} and La^{III} ions were obtained, and all the structures were determined. Fortunately, the structures of the Cu^{II}−Ln^{III} and Zn^{II}−Ln^{III} series have an isomorphous structure as well as those of the Ni^{II}−Ln^{III} and Co^{II}−Ln^{III} series. The comparison of the magnetic properties between the d−f complex with both magnetic ions and the corresponding reference complex with one diamagnetic species makes it possible to evaluate the nature of the M^{II}−Ln^{III} magnetic interactions. Alternating (ac) magnetic measurements under zero and 1000 Oe bias fields were carried out to investigate the SMM behaviors.

RESULTS AND DISCUSSION

Synthesis of M^{II}−Ln^{III} Complexes $[M^{II}(3\text{-MeOsaltn})(MeOH)_x(ac)Ln^{III}(hfac)_2]$. The present series of 3d−4f binuclear complexes was synthesized by mixing $[M(3\text{-MeOsaltn})(H_2O)_x]$ (M = Co^{II}, Ni^{II}, Cu^{II}, and Zn^{II}; 3-MeOsaltn = *N*,*N*′-bis(3-methoxy-2-oxybenzylidene)-1,3-propanediaminato) and $[Ln^{III}(ac)(Hhfac)(hfac)_2(H_2O)_2]$ (Ln = Gd^{III}, Tb^{III}, Dy^{III} and La^{III}; hfac = hexafluoroacetylacetonato, ac = acetato) as the 3d- and 4f-component complexes, respectively. This type of 3d−4f complex with the Schiff-base ligands has been studied by Gatteschi et al.[3] and Kahn et al.,[17] in which Kahn et al. used [Cu(salen)] and $[Gd(hfac)_3(H_2O)_2]$ for the d- and f-component complexes, respectively. Fukuhara et al. reported that [Cu(saltn)] (saltn = *N*,*N*′-bis(salicylidene)-1,3-diaminopropane) behaves as useful "ligand-complex" binding other d-metal ions to form tetranuclear and trinuclear complexes such as $[Cu(saltn)(\mu\text{-ac})Cu(\mu\text{-}CH_3O)_2Cu(\mu\text{-ac})(saltn)Cu]$ and $[Zn\{(\mu\text{-ac})(saltn)Cu\}_2]$.[18] Gatteschi et al. used the ligand-complex [Cu(saltn)] to prepare the Cu^{II}−Gd^{III} complex $[Cu^{II}(saltn)]_2Gd^{III}(H_2O)(NO_3)_3{\cdot}2C_2H_5NO_2$.[3b]

Scheme 1. Synthetic Scheme of Acetato- and Diphenolato-Bridged Binuclear 3d−4f Complex, $[M(3\text{-MeOsaltn})(MeOH)_x(ac)Ln(hfac)_2]$ (x = 0 for M = Cu^{II}, Zn^{II}; x = 1 for M = Co^{II}, Ni^{II}; Ln = Gd^{III}, Tb^{III}, Dy^{III} and La^{III}), by the Reaction of $[M(3\text{-MeOsaltn})(H_2O)_x]$ and $[Ln(ac)(Hhfac)(hfac)_2(H_2O)_2]$

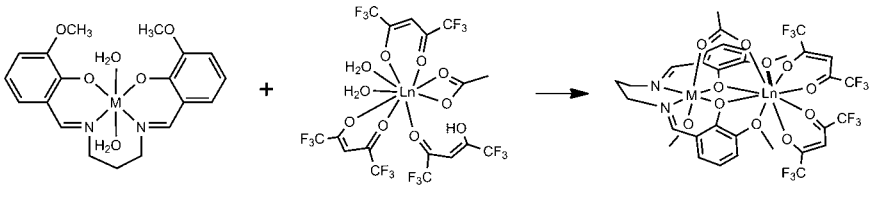

$[M^{II}(3\text{-MeOsaltn})(H_2O)_x]$ $[Ln^{III}(ac)(Hhfac)(hfac)_2(H_2O)_2]$ $[M(3\text{-MeOsaltn})(MeOH)_x(ac)Ln(hfac)_2]$

dx.doi.org/10.1021/ic400594u | *Inorg. Chem.* 2013, 52, 6160−6178

Matsumoto et al. used the modified compound [Cu(3-MeOsaltn)] for the synthesis of a series of Cu^{II}–Ln^{III} complexes.[16] He demonstrated that the d-component complexes [M(3-MeOsaltn)$(H_2O)_x$] have suitable properties for the systematic synthesis of d–f complexes with a variety of M ions of Co^{II}, Ni^{II}, Cu^{II}, and Zn^{II} as well as Fe^{III} and Mn^{III}: (1) The d-complex like [M(3-MeOsaltn)$(H_2O)_x$], that contains phenolato and the neighboring coordinating groups such as methoxy, hydroxy, and carboxy oxygen atoms,[19] can give the "ligand-complex". (2) The d-complex [M(3-MeOsaltn)$(H_2O)_x$] can give stable high-spin species with M = Co^{II} and Ni^{II} ions, while on the contrary [Ni(salen)] gives diamagnetic low-spin species. (3) The moderate solubility in common organic solvent is helpful for the reaction with f-component.[16] Recently, by the use of [Ni(3MeOsaltn)$(H_2O)_x$], Wang et al. and Pasatoiu et al. reported the syntheses and magnetic properties of the Ni^{II}–Ln^{III} complexes [Ni(3-MeOsaltn)$Ln(NO_3)_2$], which were prepared by the reaction of [Ni(3-MeOsaltn)$(H_2O)_x$] and $Ln(NO_3)_3 \cdot 4H_2O$.[20] In this study, we used the f-component complexes, [Ln^{III}(ac)(Hhfac)$(hfac)_2(H_2O)_2$] (Ln = Gd^{III}, Tb^{III}, Dy^{III} and La^{III}; hfac = hexafluoroacetylacetonato), which were prepared by the reaction of lanthanide(III) acetate tetrahydrate and hexafluoroacetylacetone with 1:3 molar ratio in water, while the f-component complex [$Ln^{III}(hfac)_3(H_2O)_2$] has been used for a number of d–f complexes.[3] Due to the stronger affinity of acetato ion to Ln^{III} ions, the f-component compounds with the formula [[Ln^{III}(ac)(Hhfac)$(hfac)_2(H_2O)_2$] were obtained. By mixing d- and f-component complexes with 1:1 molar ratio, the 3d–4f complexes were obtained as well grown crystals. The Cu^{II}–Ln^{III} and Zn^{II}–Ln^{III} complexes were obtained as green and yellow platelike crystals, respectively. The crystals of Cu^{II}–Ln^{III} and Zn^{II}–Ln^{III} complexes do not contain the solvent molecules. The Co^{II}–Ln^{III} and Ni^{II}–Ln^{III} complexes were prepared in a mixed solution of acetone and methanol in 1/1 volume and obtained as orange and blue plate crystals, respectively. The crystals of Co^{II}–Ln^{III} and Ni^{II}–Ln^{III} complexes gradually lose the crystal solvents and decompose. All the samples were dried *in vacuo* and subjected to the elemental analyses and the physical measurements. The elemental analyses agreed with the chemical formula of [M(3-MeOsaltn)$(MeOH)_x$(ac)Ln$(hfac)_2$] (x = 0 for M^{II} = Cu^{II}, Zn^{II}; x = 1 for M^{II} = Co^{II}, Ni^{II}). It should be noted that all complexes involve one acetato ion per binuclear molecular unit that bridges M^{II} and Ln^{III} ions as later confirmed by the X-ray analyses. The acetato-bridge between d- and f-ions must contribute to the stabilization of the 3d–4f binuclear complexes, and as a result a series of the d–f complexes with various d-transition metal ions is easily and successfully synthesized.

Molecular Structures of Cu^{II}–Ln^{III} and Zn^{II}–Ln^{III} (Ln^{III} = Gd^{III}, Tb^{III}, and Dy^{III}). The crystal structures were determined by single-crystal X-ray diffraction analyses at 150 K. Due to the crystal habit of the rapid decomposition and the disorder at hfac ligands, the X-ray diffraction analyses at 296 K have problems in the accuracy and the explanation of the disorder at hfac ligand. Though the basic structural information, such as an isomorphous structure for a series of Cu^{II}–Ln^{III} and Zn^{II}–Ln^{III} complexes, an acetate-bridged binuclear structure, and the coordination numbers of d- and f-elements, is undoubtedly obtained even at 296 K, the X-ray analyses at 150 K give the more reliable data. The crystallographic data of the Cu^{II}–Ln^{III} and Zn^{II}–Ln^{III} complexes (Ln^{III} = Gd^{III}, Tb^{III}, and Dy^{III}) at 150 K are listed in Table 1. All six Cu^{II}–Ln^{III} and Zn^{II}–Ln^{III} complexes crystallized in the triclinic space group $P\bar{1}$ (No. 2) with similar cell parameters, and therefore, they are isomorphous to each other. The coordination bond distances with their estimated standard deviations in parentheses are listed in Table 2, where the same atom numbering is taken for the six complexes. As the six Cu^{II}–Ln^{III} and Zn^{II}–Ln^{III} complexes are isomorphous; only the structure of the Cu^{II}–Gd^{III} complex is described in detail. Figure 1 shows the molecular structure of binuclear Cu^{II}–Gd^{III} complex with the selected atom numbering scheme. The complex has acetato- and diphenolato-bridged Cu^{II}–Gd^{III} binuclear structure with the distances of Cu···Gd = 3.4373(6) Å, Cu–O(6) = 2.231(3) Å, and Gd–O(5) = 2.327(3) Å, where O(5) and O(6) atoms of the acetate ion bridge Cu^{II} and Gd^{III} ions in a μ-acetato fashion. The Cu^{II} ion assumes a square pyramidal coordination geometry, where the equatorial coordination sites consist of N_2O_2 donor atoms of the tetradentate Schiff-base ligand (3-MeOsaltn) with the distances of Cu–O(2) = 1.969(4) Å, Cu–O(3) = 1.974(3) Å, Cu–N(1) = 1.980(4) Å, and Cu–N(2) = 1.982(5) Å, and the axial position is occupied by one of two oxygen atoms of an acetato ion with the distance of Cu–O(6) = 2.231(3) Å. The Cu^{II} ion is deviated by 0.231 Å from the equatorial N_2O_2 plane toward the oxygen atom of acetato ion. The coordination number of Gd^{III} ion is nine, consisting of four oxygen atoms of two $hfac^-$, two phenolato and two methoxy oxygen atoms of 3-MeOsaltn, and one oxygen atom of acetato ion. The Gd–O distances of two hfac ligands are Gd–O(7) = 2.443(4) Å, Gd–O(8) = 2.387(4) Å, Gd–O(9) = 2.375(4) Å, and Gd–O(10) = 2.527(3) Å. The two phenolato and two methoxy oxygen atoms of the tetradentate ligand of Cu^{II} complex coordinate to a Gd^{III} ion as the bridging atoms, with the distances of Gd–O(1) = 2.521(5) Å, Gd–O(2) = 2.388(4) Å, Gd–O(3) = 2.342(4) Å, and Gd–O(4) = 2.599(4) Å. Although the Gd–O distances from the phenolato oxygen atoms are much shorter than those from the methoxy oxygens, the bridging mode from the 3-methoxy oxygens helps to form the binuclear structure, together with the acetato-bridge. The planarity of the bridging CuO_2Gd moiety is estimated by the dihedral angle between CuO_2 and GdO_2 planes, in which the angle is 24.4°. The packing of binuclear molecules in the crystal lattice was examined (see Figure S1). The distances between the adjacent binuclear molecules are Gd···Gd = 10.1500(4) Å, Cu···Cu = 5.9522(8) Å, and Gd···Cu = 7.5770(6) Å, demonstrating that the neighboring binuclear species are well separated and thus the intermolecular magnetic interactions should be negligible.

Molecular Structures of Co^{II}–Ln^{III} and Ni^{II}–Ln^{III} (Ln^{III} = Gd^{III}, Tb^{III}, and Dy^{III}). Due to the crystal habit of the rapid decomposition and the disorder at hfac ligands, the X-ray diffraction analyses were determined at 100 K. The crystallographic data of Co^{II}–Ln^{III} and Ni^{II}–Ln^{III} (Ln^{III} = Gd^{III}, Tb^{III}, and Dy^{III}) complexes at 100 K are listed in Table 3. These six Co^{II}–Ln^{III} and Ni^{II}–Ln^{III} complexes crystallized in same monoclinic space group $P2_1/c$ (No. 14) with similar cell parameters, and they are isomorphous to each other. The coordination bond distances with their estimated standard deviations in parentheses are listed in Table 4, where the same atom numbering is taken for six complexes. As the six Co^{II}–Ln^{III} and Ni^{II}–Ln^{III} complexes are isomorphous, only the structure of Co^{II}–Gd^{III} is described in detail. Figure 2 shows the molecular structure of the binuclear Co^{II}–Gd^{III} complex with the selected atom numbering scheme. The complex has an acetato- and diphenolato-bridged heterometal binuclear structure with the distances of Co···Gd = 3.4059(5) Å, Co–O(6) = 2.082(3) Å, and Gd–O(5) = 2.349(3) Å, where the acetato ion bridges Co^{II} and Gd^{III} ions and two oxygen atoms O(5) and O(6) atoms of the acetato coordinate axially to Co^{II} and Gd^{III} ions. The Co^{II} ion assumes an octahedral coordination

dx.doi.org/10.1021/ic400594u | Inorg. Chem. 2013, 52, 6160–6178

Table 1. Crystallographic Data for the Cu^{II}–Ln^{III} and Zn^{II}–Ln^{III} Complexes $[M(3\text{-MeOsaltn})(ac)Ln(hfac)_2]$ (Ln^{III} = Gd^{III}, Tb^{III}, and Dy^{III})

	Cu^{II}–Gd^{III}	Cu^{II}–Tb^{III}	Cu^{II}–Dy^{III}
formula	$C_{31}H_{25}N_2O_{10}F_{12}CuGd$	$C_{31}H_{25}N_2O_{10}F_{12}CuTb$	$C_{31}H_{25}N_2O_{10}F_{12}CuDy$
fw	1034.32	1036.00	1039.57
cryst syst	triclinic	triclinic	triclinic
space group	$P\bar{1}$ (No. 2)	$P\bar{1}$ (No. 2)	$P\bar{1}$ (No. 2)
a/Å	10.2246(3)	10.2184(4)	10.2311(3)
b/Å	11.4639(3)	11.4642(4)	11.4571(4)
c/Å	17.5688(5)	17.5832(4)	17.5663(4)
α/deg	86.3787(9)	86.3967(8)	86.4514(11)
β/deg	75.3343(8)	75.2519(9)	75.1403(7)
γ/deg	66.2417(7)	66.2258(10)	66.1499(11)
V/Å^3	1821.59(8)	1821.06(10)	1818.23(9)
T/K	150	150	150
Z	2	2	2
D_{calcd}/g cm^{-3}	1.886	1.889	1.899
μ/cm^{-1}	25.12	26.24	27.46
R1 [$I > 2\sigma(I)$]	0.0407	0.0385	0.0417
wR2 [all data]	0.1126	0.1057	0.1219
reflns collected	17 782	17 971	17 857
unique reflns, R(int)	8242, 0.0299	8253, 0.0197	8170, 0.0270
	Zn^{II}–Gd^{III}	Zn^{II}–Tb^{III}	Zn^{II}–Dy^{III}
formula	$C_{31}H_{25}N_2O_{10}F_{12}ZnGd$	$C_{31}H_{25}N_2O_{10}F_{12}ZnTb$	$C_{31}H_{25}N_2O_{10}F_{12}ZnDy$
fw	1036.16	1037.83	1041.41
cryst syst	triclinic	triclinic	triclinic
space group	$P\bar{1}$ (No. 2)	$P\bar{1}$ (No. 2)	$P\bar{1}$ (No. 2)
a/Å	10.1860(5)	10.1697(7)	10.1959(3)
b/Å	11.5306(5)	11.5450(9)	11.5344(3)
c/Å	17.5576(8)	17.5614(14)	17.5376(5)
α/deg	86.1213(13)	86.204(3)	86.2477(8)
β/deg	75.3054(13)	75.275(3)	75.1651(8)
γ/deg	66.2677(11)	66.167(2)	66.0818(7)
V/Å^3	1824.63(14)	1822.6(3)	1820.81(8)
T/K	150	150	150
Z	2	2	2
D_{calcd}/g cm^{-3}	1.886	1.891	1.899
μ/cm^{-1}	25.82	26.97	27.47
R1 [$I > 2\sigma(I)$]	0.0387	0.0532	0.0370
wR2 [all data]	0.1203	0.1474	0.1080
reflns collected	18 003	17 277	17 892
unique reflns, R(int)	8283, 0.0362	8037, 0.0354	8228, 0.0245

geometry, where the equatorial coordination sites consist of N_2O_2 donor atoms of the tetradentate Schiff-base ligand 3-MeOsaltn with the distances of Co–O(2) = 2.058(3) Å, Co–O(3) = 2.056(2) Å, Co–N(1) = 2.063(3) Å, and Co–N(2) = 2.070(4) Å, and the two axial positions are occupied by one of two oxygen atoms of an acetato ion with the distance of Co–O(6) = 2.082(3) Å and an oxygen atom of methanol with 2.233(3) Å. The Co–N and Co–O bond distances are consistent with a high-spin state of the Co^{II} ion ($S = {}^3/_2$). On the basis of a similar examination on the coordination bond distances, also the Ni^{II} ion of the Ni^{II}–Ln^{III} complexes assumes high-spin state ($S = 1$). The coordination number of Gd^{III} ion is nine, consisting of four oxygen atoms of two $hfac^-$, two phenolato and two methoxy oxygen atoms of 3-MeOsaltn, and one oxygen atom of acetato ion. The two methoxy and two phenolato oxygen atoms of the tetradentate ligand of Co^{II} complex coordinate to a Gd^{III} ion as the bridging atoms, with the distances of Gd–O(1) = 2.706(3) Å, Gd–O(2) = 2.337(3) Å, Gd–O(3) = 2.331(3) Å, and Gd–O(4) = 2.647(3) Å. The planarity of the bridging CoO_2Gd moiety is estimated by the dihedral angle between CoO_2 and GdO_2 planes, in which the angle is 14.2°. The dihedral angle (14.2°) of the Co^{II}–Gd^{III} complex is smaller than that (24.4°) of the Cu^{II}–Gd^{III} complex, in which the Co^{II} and Cu^{II} ions have a six-coordinated octahedral and a five-coordinated square pyramidal coordination geometries, respectively. The packing manner of binuclear molecules in the crystal was examined (see Figure S2). The distances between the adjacent binuclear molecules are Gd···Gd = 9.8838(3) Å, Co···Co = 7.0791(6) Å, and Gd···Co = 7.4170(5) Å, demonstrating that the magnetic ions are well separated.

General Procedures for Magnetic Measurements of M^{II}–Ln^{III} Complexes. As the microcrystalline samples consisting of Tb^{III} and Dy^{III} ions showed reorientation in the applied magnetic field, all samples were dispersed in paraffin grease to avoid this problem, see Experimental Section. The temperature dependent magnetic susceptibility measurements on powdered samples of M^{II}–Ln^{III} were carried out in an applied magnetic field of 0.1 T in the temperature range 1.9–300 K. The field dependence of the magnetization up to 5 T was measured at 1.9 K.

dx.doi.org/10.1021/ic400594u | Inorg. Chem. 2013, 52, 6160–6178

Table 2. Coordination Bond Distances (Å) and $Ln^{III}\cdots M^{II}$ Distances (Å) for the $Cu^{II}-Ln^{III}$ and $Zn^{II}-Ln^{III}$ Complexes $[M(3\text{-MeOsaltn})(ac)Ln(hfac)_2]$ (Ln = Gd^{III}, Tb^{III}, and Dy^{III})

	$Cu^{II}-Gd^{III}$	$Cu^{II}-Tb^{III}$	$Cu^{II}-Dy^{III}$
Ln−O(1)	2.521(5)	2.515(4)	2.503(5)
Ln−O(2)	2.388(4)	2.371(3)	2.366(4)
Ln−O(3)	2.342(4)	2.327(4)	2.317(4)
Ln−O(4)	2.599(4)	2.597(4)	2.590(4)
Ln−O(5)	2.327(3)	2.310(3)	2.295(3)
Ln−O(7)	2.443(4)	2.432(4)	2.424(4)
Ln−O(8)	2.387(4)	2.368(4)	2.360(4)
Ln−O(9)	2.375(4)	2.361(3)	2.344(4)
Ln−O(10)	2.527(3)	2.507(3)	2.497(4)
Cu−O(2)	1.969(4)	1.969(4)	1.961(4)
Cu−O(3)	1.974(3)	1.980(3)	1.973(4)
Cu−O(6)	2.231(3)	2.235(3)	2.235(3)
Cu−N(1)	1.980(4)	1.986(4)	1.978(4)
Cu−N(2)	1.982(5)	1.983(5)	1.980(6)
Ln···Cu	3.4373(6)	3.4268(6)	3.4175(6)
	$Zn^{II}-Gd^{III}$	$Zn^{II}-Tb^{III}$	$Zn^{II}-Dy^{III}$
Ln−O(1)	2.548(4)	2.546(7)	2.530(5)
Ln−O(2)	2.357(3)	2.351(5)	2.338(3)
Ln−O(3)	2.323(4)	2.312(7)	2.298(4)
Ln−O(4)	2.609(4)	2.605(7)	2.606(4)
Ln−O(5)	2.376(3)	2.355(5)	2.343(3)
Ln−O(7)	2.443(4)	2.430(6)	2.423(4)
Ln−O(8)	2.391(4)	2.374(6)	2.369(4)
Ln−O(9)	2.363(3)	2.352(5)	2.339(4)
Ln−O(10)	2.515(3)	2.503(5)	2.483(3)
Zn−O(2)	2.069(4)	2.068(6)	2.061(4)
Zn−O(3)	2.062(3)	2.062(5)	2.060(3)
Zn−O(6)	1.998(3)	1.999(5)	2.003(3)
Zn−N(1)	2.064(4)	2.067(7)	2.063(4)
Zn−N(2)	2.063(5)	2.062(8)	2.062(5)
Ln···Zn	3.4499(6)	3.439(1)	3.4292(6)

The reference theoretical magnetic susceptibilities expected for the noninteracting d−f ions, using the d-ion with spin-only value and the 4f-ion with free ion approximation, have been calculated with the equation $\chi_M = \chi_{3d} + \chi_{4f}$, where $\chi_{3d} = (Ng^2\beta^2/3kT)[S(S+1)]$ and $\chi_{4f} = (Ng_J^2\beta^2/3kT)[J(J+1)]$, with $g_J = {}^3/_2 + [S(S+1) - L(L+1)]/2J(J+1)$.[21]

Magnetic Properties of $Zn^{II}-Ln^{III}$ Complexes (Ln^{III} = Gd^{III}, Tb^{III}, and Dy^{III}). The temperature dependences of the magnetic susceptibilities for the binuclear $Zn^{II}-Ln^{III}$ complexes are shown in Figure 3a, as plots of $\chi_M T$ versus T, where χ_M is the molar magnetic susceptibility per binuclear $Zn^{II}-Ln^{III}$ molecule and T is the absolute temperature. Since Zn^{II} ion with d^{10} electronic configuration is diamagnetic, the magnetic properties of the binuclear $Zn^{II}-Ln^{III}$ complexes depends only on the Ln^{III} ion and are helpful to evaluate the magnetic details for the present series of the $M^{II}-Ln^{III}$ complexes involving paramagnetic M^{II} ions. The constant $\chi_M T$ value of ca. 8.1 cm^3 K mol^{-1} over 1.9−300 K of the $Zn^{II}-Gd^{III}$ complex is reproduced by the theoretical value expected for one diamagnetic Zn^{II} ion ($3d^{10}$, $S = 0$) and a Gd^{III} ($4f^7$, $J = {}^7/_2$, $L = 0$, $S = {}^7/_2$, ${}^8S_{7/2}$) ion with $g_{Gd} = 2.028$. The $\chi_M T$ value of 12.73 cm^3 K mol^{-1} for the $Zn^{II}-Tb^{III}$ complex at 300 K is compatible with the value of 11.82 cm^3 K mol^{-1} expected for one Tb^{III} ($4f^8$, $J = 6$, $S = 3$, $L = 3$, ${}^7F_6$) ion in the free-ion approximation. On lowering the temperature, the $\chi_M T$ value decreases gradually to reach a value of 10.41 cm^3 K mol^{-1} at 1.9 K. The decrease in the lower temperature region is due to the crystal field effect on the Tb^{III} ion that removes the 13-fold degeneracy of the ${}^7F_6$ ground state.[21] The $\chi_M T$ value of 15.02 cm^3 K mol^{-1} for the $Zn^{II}-Dy^{III}$ complex at 300 K is compatible with the value of 14.17 cm^3 K mol^{-1} expected for one Dy^{III} ($4f^9$, $J = 15/2$, $S = 5/2$, $L = 5$, ${}^6H_{15/2}$) ion in the free-ion approximation. On lowering the temperature, the $\chi_M T$ value decreases gradually to 11.34 cm^3 K mol^{-1} at 1.9 K. The decrease in the lower temperature region is also due to the crystal field effect on the Dy^{III} ion that removes the 16-fold degeneracy of the ${}^6H_{15/2}$ ground state.

The field dependences of the magnetization up to 5 T for the $Zn^{II}-Ln^{III}$ complexes were measured at 1.9 K, and the $M/N\beta$ versus H plots are shown in Figure 3b. The $M/N\beta$ versus H plots of the $Zn^{II}-Gd^{III}$ complex were well reproduced by the Brillouin function for $S = {}^7/_2$ and $g = 2.06$ (the solid line) whose g-value is compatible with the value ($g = 2.028$) obtained from the magnetic susceptibility measurement. As shown in Figure 3b, upon increasing the applied external magnetic field, the magnetization of the $Zn^{II}-Tb^{III}$ complex (green triangle) increases to 5.24 $N\beta$

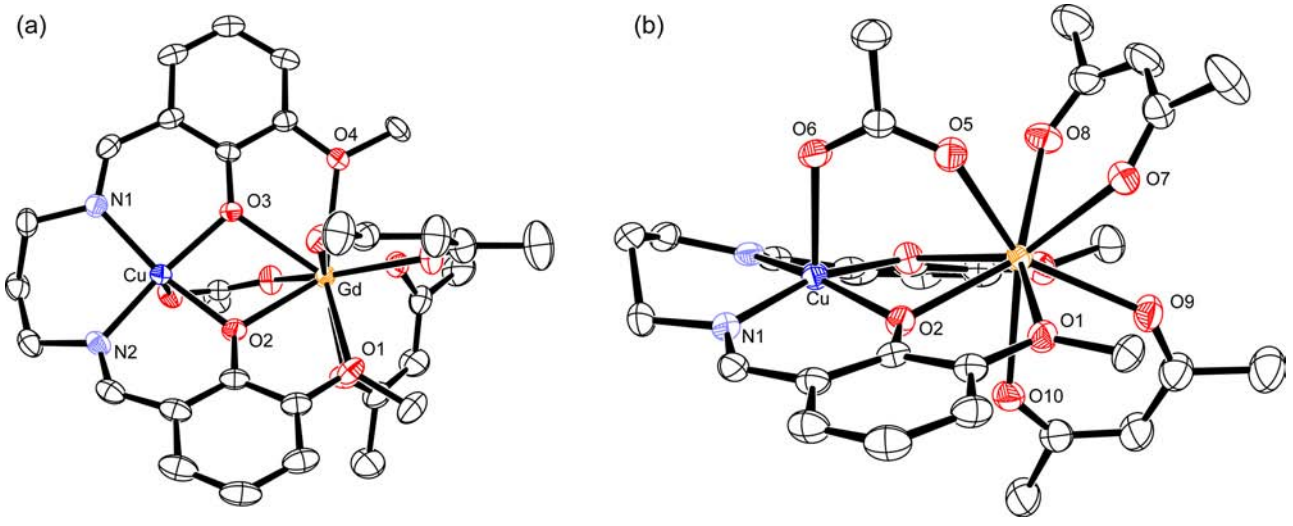

Figure 1. Molecular structure of acetato- and diphenolato-bridged binuclear $Cu^{II}-Gd^{III}$ complex with the selected atom numbering scheme. The hydrogen and fluorine atoms are omitted for clarity. (a) Perspective view projected on equatorial N_2O_2 plane. (b) Side view showing acetato-bridge.

dx.doi.org/10.1021/ic400594u | Inorg. Chem. 2013, 52, 6160−6178

Table 3. Crystallographic Data for the Ni^{II}–Ln^{III} and Co^{II}–Ln^{III} Complexes $[M(3\text{-MeOsaltn})(MeOH)(ac)Ln(hfac)_2]$ (Ln = Gd^{III}, Tb^{III}, and Dy^{III})

	Ni^{II}–Gd^{III}	Ni^{II}–Tb^{III}	Ni^{II}–Dy^{III}
formula	$C_{33}H_{33}N_2O_{12}F_{12}NiGd$	$C_{33}H_{33}N_2O_{12}F_{12}NiTb$	$C_{33}H_{33}N_2O_{12}F_{12}NiDy$
fw	1093.56	1095.24	1098.81
cryst syst	monoclinic	monoclinic	monoclinic
space group	$P2_1/c$ (No. 14)	$P2_1/c$ (No. 14)	$P2_1/c$ (No. 14)
a/Å	17.0843(7)	17.1879(6)	17.1346(4)
b/Å	12.7041(7)	12.7311(3)	12.6797(3)
c/Å	19.5631(8)	19.5571(6)	19.4864(4)
β/deg	110.2960(11)	109.4290(10)	109.7349(7)
V/ Å^3	3982.4(3)	4035.8(2)	3984.99(14)
T/K	100	100	100
Z	4	4	4
D_{caldc}/g cm^{-3}	1.824	1.802	1.831
μ/cm^{-1}	22.46	23.17	24.54
R1 [$I > 2\sigma(I)$]	0.0498	0.0395	0.0407
wR2 [all data]	0.1490	0.1040	0.1053
reflns collected	36 268	37 035	37 211
unique reflns, R(int)	9013, 0.0578	9126, 0.0287	9035, 0.0489
	Co^{II}–Gd^{III}	Co^{II}–Tb^{III}	Co^{II}–Dy^{III}
formula	$C_{33}H_{33}N_2O_{12}F_{12}CoGd$	$C_{33}H_{33}N_2O_{12}F_{12}CoTb$	$C_{33}H_{33}N_2O_{12}F_{12}CoDy$
fw	1093.79	1095.47	1099.04
cryst syst	monoclinic	monoclinic	monoclinic
space group	$P2_1/c$ (No. 14)	$P2_1/c$ (No. 14)	$P2_1/c$ (No. 14)
a/Å	17.0988(4)	17.1053(6)	17.0871(4)
b/Å	12.7846(3)	12.7743(4)	12.7293(4)
c/Å	19.6171(4)	19.6165(5)	19.5855(5)
β/deg	110.0599(7)	110.0478(9)	110.0456(7)
V/Å^3	4028.17(14)	4026.64(19)	4001.92(16)
T/K	100	100	100
Z	4	4	4
D_{calcd}/g cm^{-3}	1.803	1.807	1.824
μ/cm^{-1}	21.65	22.67	23.87
R1 [$I > 2\sigma(I)$]	0.0371	0.0379	0.0377
wR2 [all data]	0.0937	0.0949	0.0908
reflns collected	37 618	36 152	37 542
uniq reflns, R(int)	9175, 0.0352	9154, 0.0429	9033, 0.0313

at 5 T but did not reach the expected saturation value (9 $N\beta$ for the Tb^{III} ion). This is due to the crystal field effect on the Tb^{III} ion. The highest of the levels into which the $^7F_6$ state is split do not contribute to the magnetization, which therefore does not reach the saturation value. This effect is well-known for transition metal ions with a significant zero-field-splitting and also applied to rare earth ions except for Gd^{III} ion which has an isotropic ground $^8S_{7/2}$ state. As shown in Figure 3b, upon increasing the applied external magnetic field, the magnetization of the Zn^{II}–Dy^{III} complex increases to 5.59 $N\beta$ at 5 T but did not reach the expected saturation value (10 $N\beta$ for the Dy^{III} ion). This is also due to the crystal field effect on the Dy^{III} ion.

Magnetic Properties of Cu^{II}–Ln^{III} Complexes (Ln^{III} = Gd^{III}, Tb^{III}, and Dy^{III}). The temperature dependences of the magnetic susceptibilities for the binuclear Cu^{II}–Ln^{III} complexes are shown in Figure 4a. The $\chi_M T$ value of 8.81 cm^3 K mol^{-1} at 300 K of the Cu^{II}–Gd^{III} complex is compatible with the theoretical value of 8.25 cm^3 K mol^{-1} expected for a Cu^{II} ($3d^9$, $S = {}^1/_2$) and a Gd^{III} ($4f^7$, $S = {}^7/_2$) noninteracting ions. On lowering temperature, the $\chi_M T$ value increases gradually to the value of 10.59 cm^3 K mol^{-1} at 1.9 K. The increase of the $\chi_M T$ value indicates an intramolecular ferromagnetic interaction between Cu^{II} and Gd^{III} ions. The value of $\chi_M T$ = 10.59 cm^3 K mol^{-1} at 1.9 K is compatible with the value of 10.00 cm^3 K mol^{-1}, expected for an isolated S = 4 spin state resulting from ferromagnetic coupling between the Cu^{II} ($S = {}^1/_2$) and Gd^{III} ($S = {}^7/_2$) ions assuming $g_{Cu} = g_{Gd}$ = 2.00. Fits to the experimental data were performed assuming for the Gd^{III} ion an isotropic $^8S_{7/2}$ state without orbital angular momentum and using the following spin Hamiltonian, $H = g_{Cu}\beta S_{Cu}H + g_{Gd}\beta S_{Gd}H - 2J(Cu{-}Gd)S_{Cu}\cdot S_{Gd}$ in which g_{Gd} and g_{Cu} are the g factors for the Gd^{III} and Cu^{II} ions, H is the applied field, and J is the Heisenberg coupling constant between the two ions, respectively. The solid line in Figure 4a shows the theoretical curve with the best fit parameters of g_{Cu} = 2.17, g_{Gd} = 2.03, J(Cu–Gd) = +2.6 cm^{-1}, being consistent with an intramolecular ferromagnetic interaction between the Cu^{II} and Gd^{III} ions and a negligible weak intermolecular antiferromagnetic interaction.

The $\chi_M T$ value of 12.76 cm^3 K mol^{-1} for Cu^{II}–Tb^{III} complex at 300 K is compatible with the value of 12.19 cm^3 K mol^{-1} expected for one Cu^{II} and one Tb^{III} magnetically isolated ions. On lowering the temperature, the $\chi_M T$ value decreases gradually to 12.05 cm^3 K mol^{-1} at 10.0 K and then decreases abruptly. The $\chi_M T$ value of 15.18 cm^3 K mol^{-1} for the Cu^{II}–Dy^{III} complex at 300 K is comparable with the value of 14.54 cm^3 K mol^{-1} expected for one Cu^{II} and one Dy^{III} magnetically isolated ions. On lowering the temperature, the $\chi_M T$ value decreases gradually

dx.doi.org/10.1021/ic400594u | Inorg. Chem. 2013, 52, 6160–6178

Table 4. Coordination Bond Distances (Å) and $Ln^{III}\cdots M^{II}$ Distances (Å) for the $Ni^{II}-Ln^{III}$ and $Co^{II}-Ln^{III}$ Complexes $[M(3\text{-MeOsaltn})(MeOH)(ac)Ln(hfac)_2]$ (Ln = Gd^{III}, Tb^{III}, and Dy^{III})

	$Ni^{II}-Gd^{III}$	$Ni^{II}-Tb^{III}$	$Ni^{II}-Dy^{III}$
Ln−O(1)	2.690(4)	2.703(4)	2.699(4)
Ln−O(2)	2.335(4)	2.319(3)	2.309(3)
Ln−O(3)	2.324(4)	2.311(4)	2.298(4)
Ln−O(4)	2.639(4)	2.642(3)	2.632(4)
Ln−O(5)	2.340(4)	2.336(3)	2.312(3)
Ln−O(8)	2.386(5)	2.369(4)	2.354(4)
Ln−O(9)	2.423(4)	2.410(3)	2.404(3)
Ln−O(10)	2.368(4)	2.362(3)	2.338(3)
Ln−O(11)	2.462(4)	2.458(3)	2.440(3)
Ni−O(2)	2.040(4)	2.047(4)	2.043(4)
Ni−O(3)	2.036(4)	2.037(3)	2.038(3)
Ni−O(6)	2.066(4)	2.063(3)	2.056(3)
Ni−O(7)	2.185(4)	2.172(3)	2.172(4)
Ni−N(1)	2.026(4)	2.034(4)	2.024(4)
Ni−N(2)	2.031(5)	2.038(4)	2.035(5)
Ln···Ni	3.4009(7)	3.3985(5)	3.3839(5)
	$Co^{II}-Gd^{III}$	$Co^{II}-Tb^{III}$	$Co^{II}-Dy^{III}$
Ln−O(1)	2.706(3)	2.714(3)	2.714(4)
Ln−O(2)	2.337(3)	2.324(3)	2.310(3)
Ln−O(3)	2.331(3)	2.314(3)	2.300(3)
Ln−O(4)	2.647(3)	2.647(3)	2.646(3)
Ln−O(5)	2.349(3)	2.335(3)	2.321(3)
Ln−O(8)	2.387(4)	2.369(4)	2.355(4)
Ln−O(9)	2.427(3)	2.412(3)	2.403(3)
Ln−O(10)	2.376(3)	2.356(3)	2.342(3)
Ln−O(11)	2.461(3)	2.454(3)	2.444(3)
Co−O(2)	2.058(3)	2.060(3)	2.063(3)
Co−O(3)	2.056(2)	2.060(2)	2.052(3)
Co−O(6)	2.082(3)	2.083(3)	2.089(3)
Co−O(7)	2.233(3)	2.232(3)	2.228(3)
Co−N(1)	2.063(3)	2.063(3)	2.059(4)
Co−N(2)	2.070(4)	2.070(4)	2.065(4)
Ln···Co	3.4059(5)	3.3980(5)	3.3827(5)

to reach a minimum value of 14.07 cm^3 K mol^{-1} at 26.0 K, and then increases, finally showing a small decrease at the lowest temperatures. The magnetic behavior at low temperatures of these two complexes comes from the interplay of two effects: (1) a magnetic interaction between the Cu^{II} and Ln^{III} ions and (2) a crystal field splitting of the Tb^{III} or Dy^{III} ion. The latter effect leads to a decrease of the $\chi_M T$ value in the lower temperature region, as seen for the $Zn^{II}-Tb^{III}$ and $Zn^{II}-Dy^{III}$ complexes where it is the only one to operate. The former effect leads to an increase of $\chi_M T$ if the magnetic interaction is ferromagnetic. The increase of the $\chi_M T$ value in the low temperature region for the $Cu^{II}-Dy^{III}$ complex suggests that a ferromagnetic interaction prevails against the effect of the crystal field splitting, while a less clear situation occurs for the $Cu^{II}-Tb^{III}$ complex for which the two effects seem to compensate and the $\chi_M T$ value shows a plateau in the low temperature region before decreasing below 10 K.

The field dependences of the magnetization up to 5 T for the $Cu^{II}-Ln^{III}$ complexes were measured at 1.9 K, and the $M/N\beta$ vs H plots are shown in Figure 4b. The $M/N\beta$ versus H plots of the $Cu^{II}-Gd^{III}$ complex were well reproduced by the Brillouin function for $S = 4$ and $g = 2.09$ (the solid line). Therefore, the curve fitting of the magnetization as well as that of the magnetic susceptibility indicates clearly that the $Cu^{II}-Gd^{III}$ complex has an isolated $S = 4$ spin ground state resulting from the ferromagnetic interaction between Cu^{II} ($S = {}^1/_2$) and Gd^{III} ($S = {}^7/_2$) ions. Indeed, using the value of $J(Cu-Gd) = +2.6$ cm^{-1} from the magnetic susceptibility analysis, the $S = 3$ excited state is 20.8 cm^{-1} ($8J$) above the $S = 4$ ground state and is not populated at the temperature of 1.9 K at which the magnetization data have been measured.

As shown in Figure 4b, upon increasing the applied external magnetic field, the magnetization of the $Cu^{II}-Tb^{III}$ complex (green triangle) increased to 6.65 $N\beta$ at 5 T but did not reach the expected saturation value (9 $N\beta$ for the Tb^{III} ion and 1 $N\beta$ for the Cu^{II} ion). This is due to the crystal field effect on the Tb^{III} ion. Upon increasing the applied external magnetic field, the magnetization of the $Cu^{II}-Dy^{III}$ complex increased to 6.23 $N\beta$ at 5 T but did not reach the expected saturation value (10 $N\beta$ for the

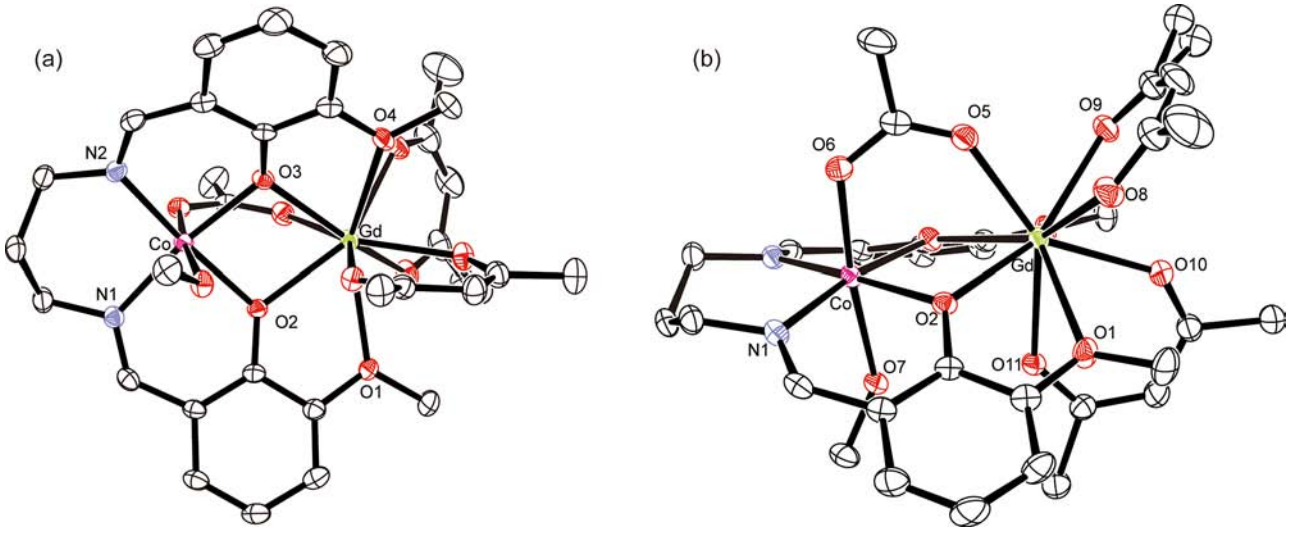

Figure 2. Molecular structure of acetate- and diphenolato-bridged binuclear $Co^{II}-Gd^{III}$ complex with the selected atom numbering scheme. The Co^{II} ion assumes octahedral coordination geometry with equatorial tetradentate ligand and acetato and methanol oxygens. The hydrogen and fluorine atoms and solvent molecule are omitted for clarity. (a) Perspective view projected on equatorial N_2O_2 plane. (b) Side view showing acetate-bridge and coordination of methanol to Co.

dx.doi.org/10.1021/ic400594u | Inorg. Chem. 2013, 52, 6160−6178

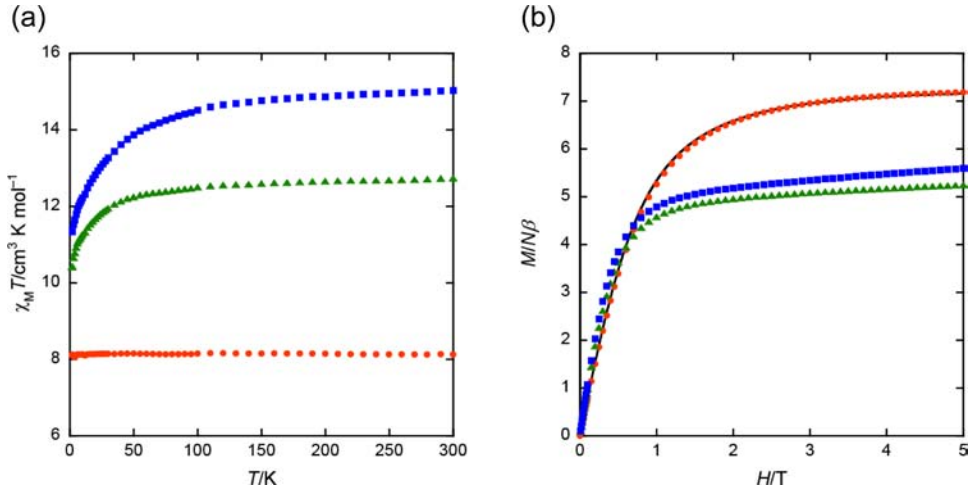

Figure 3. (a) Plots of $\chi_M T$ vs T for binuclear Zn^{II}–Ln^{III} complexes [Ln^{III} = Gd^{III} (red), Tb^{III} (green), and Dy^{III} (blue)]. (b) Field dependence of the magnetization for the Zn^{II}–Ln^{III} complexes [Ln^{III} = Gd^{III} (red), Tb^{III} (green), and Dy^{III} (blue)] at 1.9 K, as plots of $M/N\beta$ vs H. The solid line of the Zn^{II}–Gd^{III} complex represents the theoretical curve of $M = Ng\beta SB_S(y)$ for $g = 2.06$ and $S = {}^7/_2$.

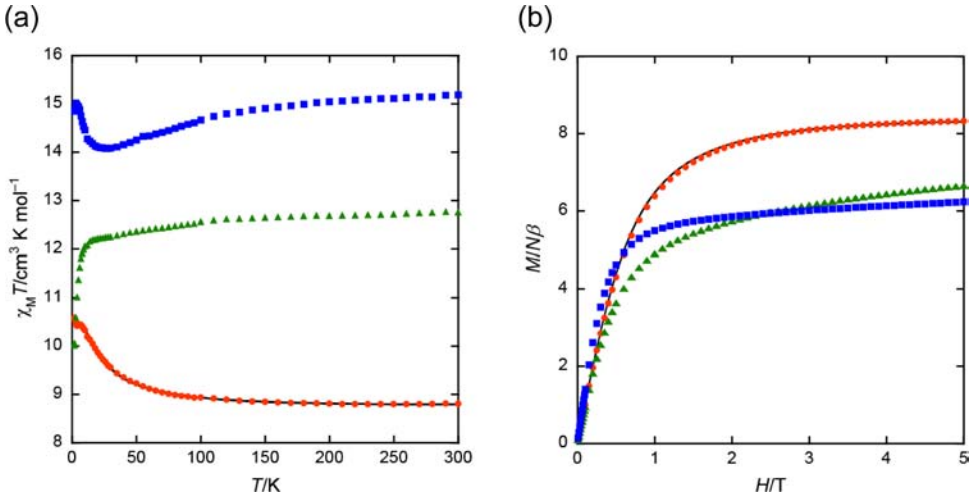

Figure 4. (a) Plots of $\chi_M T$ vs T for binuclear Cu^{II}–Ln^{III} complexes [Ln^{III} = Gd^{III} (red), Tb^{III} (green), and Dy^{III} (blue)]. The solid line of the Cu^{II}–Gd^{III} complex represents the theoretical curve for Cu^{II}–Gd^{III} complex with the best fit parameters of $g_{Cu} = 2.17$, $g_{Gd} = 2.03$, J(Cu–Gd) = +2.6 cm^{-1}. (b) Field dependence of the magnetization for the Cu^{II}–Ln^{III} complexes [Ln^{III} = Gd^{III} (red), Tb^{III} (green), and Dy^{III} (blue)] at 1.9 K, as plots of $M/N\beta$ vs H. The solid line of the Cu^{II}–Gd^{III} complex represents the theoretical curve for $g = 2.09$ and $S = 4$ spin state produced by ferromagnetic coupling between Cu^{II} ($S = {}^1/_2$) and Gd^{III} ($S = {}^7/_2$) ions.

Dy^{III} ion and 1 $N\beta$ for the Cu^{II} ion). This is also due to the crystal field effect on the Dy^{III} ion. These results demonstrate that the Cu^{II}–Dy^{III} complex has a large magnetic moment and a magnetic anisotropy in the same manner as the Cu^{II}–Tb^{III} complex.

Magnetic Properties of Ni^{II}–Ln^{III} Complexes (Ln^{III} = La^{III}, Gd^{III}, Tb^{III}, and Dy^{III}). The temperature dependences of magnetic susceptibilities are shown in Figure 5a, as plots of $\chi_M T$ versus T. The constant $\chi_M T$ value of ca. 1.2 cm^3 K mol^{-1} over 20–300 K of the Ni^{II}–La^{III} complex is reproduced by the theoretical value expected for a Ni^{II} ($3d^8$, $S = 1$) ion with $g_{Ni} = 2.2$ and one diamagnetic La^{III} ion ($4f^0$). On lowering the temperature, the $\chi_M T$ value decreases gradually to reach a value of 0.40 cm^3 K mol^{-1} at 1.9 K. The decrease in the lower temperature region is due to the zero-field-splitting (ZFS) of Ni^{II} ion. Fits to the experimental data were performed using the spin Hamiltonian β, $H = g_{Ni}\beta S_{Ni}H + D_{Ni}[S_z{}^2{}_{Ni} - S(S+1)/3]$ in which g_{Ni} is the g factor for the Ni^{II} ion, H is the applied field, $S = 1$ is the Ni^{II} spin number, and D_{Ni} is the ZFS parameter for Ni^{II}. A good fit was obtained for $g_{Ni} = 2.21$ and $D_{Ni} = +8.6$ cm^{-1}, both parameters being in the range of values measured for other Ni^{II} complexes.[20b]

The $\chi_M T$ value of the Ni^{II}–Gd^{III} complex is 9.78 cm^3 K mol^{-1} at 300 K, which is compatible with the calculated value of 8.88 cm^3 K mol^{-1} expected for a high spin Ni^{II} ($S = 1$) and a Gd^{III} ($S = {}^7/_2$) noninteracting ions. On lowering temperature, the $\chi_M T$ value increases gradually to reach a maximum value of 12.59 cm^3 K mol^{-1} at 3.0 K. The increase indicates an intramolecular ferromagnetic interaction between Ni^{II} and Gd^{III} ions while the very slight decrease below 3 K can be ascribed to a zero-field-splitting of the Ni^{II}, as suggested by the analysis of the magnetic data for the Ni^{II}–La^{III} complex, see above. The maximum value of 12.59 cm^3 K mol^{-1} at 3.0 K is close to the value of 12.38 cm^3 K mol^{-1} expected for an isolated $S = {}^9/_2$ spin state resulting from ferromagnetic coupling between the Ni^{II} ($S = 1$) and Gd^{III} ($S = {}^7/_2$) ions of the binuclear complex. Fits to the experimental data were performed assuming for the Gd^{III} ion an isotropic ${}^8S_{7/2}$ state and using the following spin Hamiltonian, $H = g_{Ni}\beta S_{Ni}H + g_{Gd}\beta S_{Gd}H + D_{Ni}[S_z{}^2{}_{Ni} - S(S+1)/3] - 2J(\text{Ni–Gd})S_{Ni}\cdot S_{Gd}$ in

dx.doi.org/10.1021/ic400594u | Inorg. Chem. 2013, 52, 6160–6178

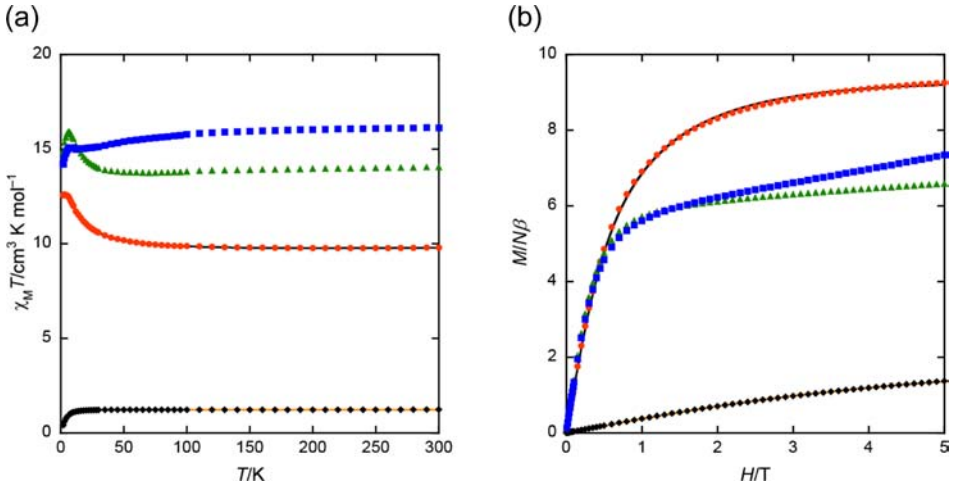

Figure 5. (a) Plots of $\chi_M T$ vs T for the Ni^{II}–Ln^{III} complexes [Ln^{III} = Gd^{III} (red), Tb^{III} (green), Dy^{III} (blue), and La^{III}(black)]. The orange solid line represents the theoretical curve for the Ni^{II}–La^{III} complex with the best fit parameters of g_{Ni} = 2.21 and D_{Ni} = +8.6 cm^{-1}. The black solid line represents the theoretical curve for the Ni^{II}–Gd^{III} complex with the best fit parameters of g_{Ni} = 2.20, g_{Gd} = 2.00, J(Ni–Gd) = +1.1 cm^{-1}, D = +7.1 cm^{-1}. (b) Field dependence of the magnetization at 1.9 K for Ni^{II}–Ln^{III} complexes [Ln^{III} = Gd^{III} (red), Tb^{III} (green), Dy^{III} (blue), and La^{III} (black)].The solid line for the Ni^{II}–La^{III} complex represents the theoretical curve with the best fit parameters of g_{Ni} = 2.28, D_{Ni} = 5.1 cm^{-1}. The black solid line for the Ni^{II}–Gd^{III} complex represents the theoretical curve with the best-fit parameters of $g_{9/2}$ = 2.06, $D_{9/2}$ = +0.16 cm^{-1}.

which g_{Ni} and g_{Gd} are the g factors for the Ni^{II} and Gd^{III} ions, H is the applied field, D_{Ni} is the ZFS parameter for Ni^{II}, and J(Ni–Gd) is the Heisenberg coupling constant between the two ions. The inclusion of the ZFS term is required to reproduce the experimental data and is consistent with the analysis of the magnetization data, see below. The best-fit parameters to the data were g_{Gd}= 2.04, g_{Ni}= 2.20, J(Ni–Gd) = +1.1 cm^{-1}, D_{Ni} = +7.1 cm^{-1}, with the values for g_{Ni} and D_{Ni} being compatible with the analysis of the magnetic data for the Ni^{II}–La^{III} complex, see above. The calculated J(Ni–Gd) value is lower than that reported by Costes et al. for a Ni^{II}–Gd^{III} binuclear complex with two phenolato bridges of J = +3.6 cm^{-1},[22] but slightly larger than the value observed by Chen et al. for a Ni^{II}–Gd^{III} compound with three phenolato bridges, which had J = +0.56 cm^{-1}.[23]

The $\chi_M T$ value of 14.05 cm^3 K mol^{-1} at 300 K for the Ni^{II}–Tb^{III} complex is slightly higher than the value of 12.82 cm^3 K mol^{-1} expected for one Ni^{II} (S = 1) and one Tb^{III} (4f^8, J = 6, S = 3, L = 3, $^7F_6$) magnetically isolated ions. On lowering the temperature, the $\chi_M T$ value increases gradually to reach a maximum value of 15.89 cm^3 K mol^{-1} at 6.0 K and then decreases abruptly. The $\chi_M T$ value of 16.12 cm^3 K mol^{-1} at 300 K for the Ni^{II}–Dy^{III} complex is also slightly higher than the value of 15.17 cm^3 K mol^{-1} expected for one Ni^{II} (S = 1) and one Dy^{III} (4f^9, J = 15/2, S = 5/2, L = 5, $^6H_{15/2}$) magnetically isolated ions, and the $\chi_M T$ value decreases gradually with decreasing temperature to 14.98 cm^3 K mol^{-1} at 12.0 K and then barely increases to 15.07 cm^3 K mol^{-1} at 7.0 K, before finally decreaseing abruptly.

The field dependences of the magnetization for the Ni^{II}–Ln^{III} complexes (Ln^{III} = La^{III}, Gd^{III}, Tb^{III}, and Dy^{III}) were measured at 1.9 K, and the $M/N\beta$ versus H curve is shown in Figure 5b. We see that the magnetization $M/N\beta$ for the Ni^{II}–La^{III} complex assumes values much lower than those expected from the Brillouin function for an S = 1 ground state: this is due to the strong zero field splitting, which leads to a split the S = 1 ground state into two M_S = 0, ± 1 components, preventing the magnetization from reaching the saturation value of g_S with S = 1. The correct dependence of the magnetization as a function of the field H can be obtained through the full-matrix diagonalization of the Hamiltonian matrix, using the three spin functions of the S = 1 state and the Hamiltonian used for the fit of the magnetic susceptibility, see above. The best fit, shown as a solid line in the lower part of the Figure 5b, was obtained for g_{Ni}=2.28, and D_{Ni} = 5.1 cm^{-1}, values compatible with those obtained from the fit of $\chi_M T$.

The data of the Ni^{II}–Gd^{III} complex are only qualitatively reproduced by Brillouin curves for S = $^9/_2$ with g = 2.03, demonstrating the presence of an isolated S = $^9/_2$ spin ground state derived from the ferromagnetic coupling between Ni^{II} (S = 1) and Gd^{III} (S = $^7/_2$) ions. Indeed, using the value of J(Ni–Gd) = +1.1 cm^{-1} from the magnetic susceptibility analysis, the lowest S = $^7/_2$ excited state is 9.9 cm^{-1} (9J) above the S = $^9/_2$ ground state and is thus not significantly populated at the temperature of 1.9 K at which the magnetization data have been measured. The data are quantitatively simulated including a ZFS term in the Hamiltonian β, H = $g_{9/2}\beta SH + D_{9/2}[S_z^2 - S(S+1)/3]$ in which $g_{9/2}$ and $D_{9/2}$ are the g factor and the ZFS parameters for the S = $^9/_2$ state, and the best fit to the experimental data yields the following values: $g_{9/2}$ = 2.06 and $D_{9/2}$ = +0.16 cm^{-1} (see solid line in the upper part of Figure 5b). It is worth noting that the $D_{9/2}$ value obtained from the fit of the magnetization data refers to the S = $^9/_2$ state and can be compared with the single ion value of D_{Ni} = +5.1 cm^{-1} for Ni^{II} obtained from a fit of the magnetization for the Ni^{II}–La^{III} complex using the Wigner–Eckart theorem.[24] For instance, using eqs 6.4.3 and 6.4.4 of ref 24 and taking into account that the ZFS of the Gd^{III} ion is negligible, it can be shown that $D_{9/2}$ = (1/36)D_{Ni}. This justifies, at least qualitatively, the smaller value of $D_{9/2}$, by over 1 order of magnitude.

As shown in Figure 5b, upon increasing the applied external magnetic field, the magnetization of Ni^{II}–Tb^{III} complex increases up to 6.58 $N\beta$ at 5 T but does not reach the expected saturation value of 11 $N\beta$ (9 $N\beta$ for Tb^{III} ion and 2 $N\beta$ for Ni^{II} ion). This is due to the crystal field effect on the Tb^{III} ion. The magnetization of Ni^{II}–Dy^{III} complex increases to 7.34 $N\beta$ at 5 T but does not reach the expected saturation value of 12 $N\beta$ (10 $N\beta$ for Dy^{III} ion and 2 $N\beta$ for Ni^{II} ion), also due to the crystal field effect on the Dy^{III} ion.

Magnetic Properties of the Co^{II}–Ln^{III} Complexes (Ln^{III} = La^{III}, Gd^{III}, Tb^{III}, and Dy^{III}). The temperature dependences of

dx.doi.org/10.1021/ic400594u | Inorg. Chem. 2013, 52, 6160–6178

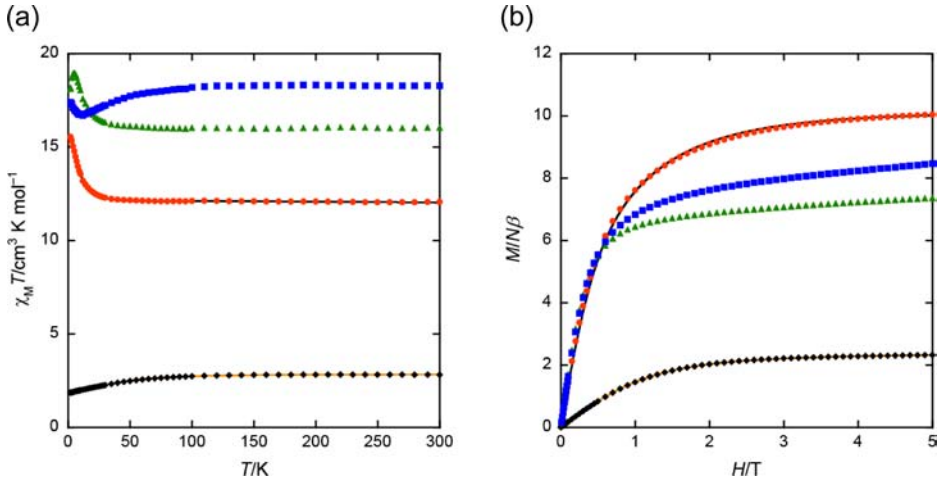

Figure 6. (a) Plots of $\chi_M T$ vs T for the Co^{II}–Ln^{III} complexes [Ln^{III} = Gd^{III} (red), Tb^{III} (green), Dy^{III} (blue), and La^{III} (black)]. The orange line for the Co^{II}–La^{III} complex represents the theoretical curve with the parameters of g_{Co} = 2.46, D_{Co} = +42 cm^{-1}. The black solid line represents the theoretical curve for the Co^{II}–Gd^{III} complex with the best fit parameters of g_{Co} = 2.59, g_{Gd} = 2.09, J(Co–Gd) = +0.60 cm^{-1}, and D = +51 cm^{-1}. (b) Field dependence of the magnetization at 1.9 K for Co^{II}–Ln^{III} complexes [Ln^{III} = Gd^{III} (red), Tb^{III} (green), Dy^{III} (blue), and La^{III} (black)]. The solid line for the Co^{II}–La^{III} complex represents the theoretical curves with g_{Co} = 2.59, D_{Co} = +49 cm^{-1}. The solid line for the Co^{II}–Gd^{III} complex represents the theoretical curve for the best fit parameters of g_S = 2.03, D_S = 0.14 cm^{-1} for the S = 5 ground state of the Co^{II}–Gd^{III} complex.

magnetic susceptibilities for the Co^{II}–Ln^{III} complexes (Ln^{III} = La^{III}, Gd^{III}, Tb^{III}, and Dy^{III}) are shown in Figure 6a. The constant $\chi_M T$ value of ca. 2.81 cm^3 K mol^{-1} over 120–300 K of the Co^{II}–La^{III} complex is reproduced by the theoretical value expected for a high spin Co^{II} (3d^7, S = $^3/_2$) ion with g_{Co} = 2.45 and one diamagnetic La^{III} ion (4f^0). On lowering the temperature, the $\chi_M T$ value keeps constant in the temperature range 120–300 K and then decreases gradually to reach a value of 1.86 cm^3 K mol^{-1} at 1.9 K. The decrease in the lower temperature region is due to a large zero-field-splitting (ZFS) of Co^{II} ion. An isotropic spin Hamiltonian is not strictly applicable to octahedral Co^{II} complexes because of the strong spin–orbit splitting of the $^4T_{1g}$ ground term but can be employed to distorted octahedral geometries where the orbital degeneracy of the $^4T_{1g}$ state is removed. Indeed, the experimental data for the Co^{II}–La^{III} complex could be fitted using the spin Hamiltonian, $H = g_{Co}\beta S_{Co}H + D_{Co}[S_z^2{}_{Co} - S(S+1)/3]$ in which g_{Co} is the g factor for the Co^{II} ion, H is the applied field, S = $^3/_2$ is the Co^{II} spin number, and D_{Co} is the ZFS parameter for Co^{II}. The best-fit parameters to the data were g_{Co}= 2.46 and D_{Co} = +42 cm^{-1}. Although quite high, the calculated ZFS parameter D_{Co} is in the range of values measured for other Co^{II} complexes with a N_2O_4 coordination.[25]

The $\chi_M T$ value of the Co^{II}–Gd^{III} complex is 12.06 cm^3 K mol^{-1} at 300 K, which is higher than the calculated value of 9.75 cm^3 K mol^{-1} expected for a high spin Co^{II} (3d^7, S = $^3/_2$) and a Gd^{III} (4f^7, J = $^7/_2$, L = 0, S = $^7/_2$, $^8S_{7/2}$) noninteracting ions. On lowering temperature, the $\chi_M T$ value increases gradually to a value of 15.54 cm^3 K mol^{-1} at 1.9 K. The increase indicates an intramolecular ferromagnetic interaction between Co^{II} and Gd^{III} ions. Fits to the experimental data were performed assuming for the Gd^{III} ion an isotropic $^8S_{7/2}$ state without orbital angular momentum and using the following spin Hamiltonian, $H = g_{Co}\beta S_{Co}H + g_{Gd}\beta S_{Gd}H + D_{Co}[S_z^2{}_{Co} - S(S+1)/3] - 2J(\text{Co–Gd})\text{-}S_{Co}\cdot S_{Gd}$ in which g_{Co} and g_{Gd} are the g factors for the Co^{II} and Gd^{III} ions, H is the applied field, D_{Co} is the ZFS parameter for Co^{II}, and J is the Heisenberg coupling constant between the two ions. Although not necessarily required by a decrease of the $\chi_M T$ value in low temperature region, a ZFS term has been added as suggested by the data for the Co^{II}–La^{III} complex and to improve the fitting. The best-fit parameters to the data were g_{Gd}= 2.09, g_{Co}= 2.59, J(Co–Gd) = +0.6 cm^{-1}, and D_{Co} = +51 cm^{-1} with g_{Co} and D_{Co} values close to those obtained for the Co^{II}–La^{III} complex, see above. The calculated J(Co–Gd) value is slightly lower than that reported by Costes et al.[26] for a Co^{II}–Gd^{III}, binuclear complex with two phenolato bridges of J = +0.90 cm^{-1}, the only magnetic coupling constant between Co^{II} and Gd^{III} ions, to the best of our knowledge.

The $\chi_M T$ value of 16.04 cm^3 K mol^{-1} at 300 K for the Co^{II}–Tb^{III} complex is higher than the value of 13.69 cm^3 K mol^{-1} expected for one Co^{II} (S = $^3/_2$) and one Tb^{III} magnetically isolated ions. On lowering the temperature, the $\chi_M T$ value increases gradually to reach a value of 18.97 cm^3 K mol^{-1} at 5.0 K and then decreases. The $\chi_M T$ value of 18.29 cm^3 K mol^{-1} at 300 K for the Co^{II}–Dy^{III} complex is higher than the value of 16.05 cm^3 K mol^{-1} expected for one Co^{II} (S = $^3/_2$) and one Dy^{III} magnetically isolated ions. On lowering the temperature, the $\chi_M T$ value decreases gradually to reach a minimum value of 16.68 cm^3 K mol^{-1} at 12.0 K, and then increases to 17.38 cm^3 K mol^{-1} at 1.9 K.

The field dependences of the magnetization for the Co^{II}–Ln^{III} complexes (Ln^{III} = La^{III}, Gd^{III}, Tb^{III}, and Dy^{III}) were measured at 1.9 K, and the $M/N\beta$ versus H curve is shown in Figure 6b. The magnetization $M/N\beta$ for the Co^{II}–La^{III} complex assumes values much lower than those expected from the Brillouin function for an S = $^3/_2$ ground state, due to the strong zero field splitting. The correct dependence of the magnetization as a function of the field H can be obtained through the full-matrix diagonalization of the Hamiltonian matrix, using the four spin functions of the S = $^3/_2$ state and the Hamiltonian used for the fit of the magnetic susceptibility, see above. The best fit, as shown in the lower part of the Figure 6b, was obtained for g_{Co} = 2.59, and D_{Co} = +49 cm^{-1}, whose values are compatible with those obtained from the fit of $\chi_M T$ versus T.

The data for the Co^{II}–Gd^{III} complex are only qualitatively reproduced by Brillouin curves for S = 5 and g = 1.99, demonstrating the presence of an isolated S = 5 spin ground state derived from the ferromagnetic coupling between Co^{II} (S = $^3/_2$) and Gd^{III} (S = $^7/_2$) ions. Indeed, using the value of J(Co–Gd) = +0.6 cm^{-1} from the magnetic susceptibility analysis, the lowest S = 4 excited state is 6.0 cm^{-1} (10J) above the S = 5 ground state and is thus

dx.doi.org/10.1021/ic400594u | Inorg. Chem. 2013, 52, 6160–6178

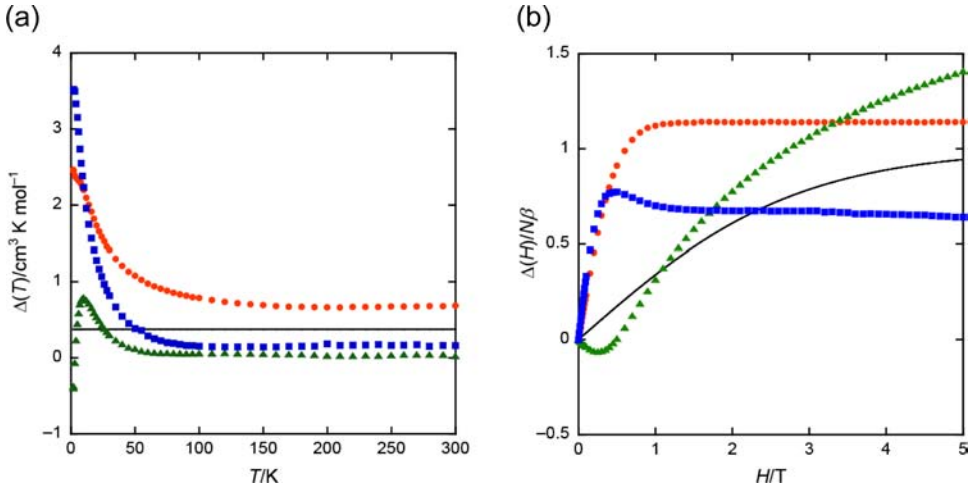

Figure 7. (a) Plots of $\Delta(T) = (\chi_M T)_{CuLn} - (\chi_M T)_{ZnLn}$ vs temperature T for the Cu^{II}–Ln^{III} complexes [Ln^{III} = Gd^{III} (red), Tb^{III} (green), and Dy^{III} (blue)] and theoretical value of one Cu^{II} ion (−). (b) Plots of $\Delta(H) = M_{CuLn}(H) - M_{ZnLn}(H)$ vs magnetic field H for the Cu^{II}–Ln^{III} complexes [Ln^{III} = Gd^{III} (red), Tb^{III} (green), and Dy^{III}(blue)]. Black solid line is the theoretical magnetization curve (Brillouin functions) of an independent Cu^{II} ions with $S = {}^1/_2$ and $g = 2.00$.

barely populated at the temperature of 1.9 K at which the magnetization data have been measured. The data are quantitatively simulated including a ZFS term in the Hamiltonian β, $H = g_5\beta SH + D_5[S_z^2 - S(S+1)/3]$ in which g_5 and D_5 are the g factor and the ZFS parameters for the $S = 5$ state, and the best fit to the experimental data yields the following values: $g_5 = 2.03$ and $D_5 = +0.14$ cm^{-1} (see solid line in the upper part of Figure 6b). As already seen for the Ni^{II}–Gd^{III} complex, the D_5 value obtained from the fit of the magnetization data is related to the single ion value of $D_{Co} = +49$ cm^{-1} for Co^{II} obtained from a fit of the magnetization for the Co^{II}–La^{III} complex using the Wigner–Eckart theorem.[24] It can be shown that $D_5 = (1/30)D_{Co}$, thus justifying, at least qualitatively, the smaller value of D_5, by almost 2 orders of magnitude.

As shown in Figure 6b, upon increasing the applied external magnetic field, the magnetizations of Co^{II}–Tb^{III} and Co^{II}–Dy^{III} complexes are increased to 7.36 and 8.47 $N\beta$ at 5 T, respectively, but did not reach the expected saturation values of 12 $N\beta$ (9 $N\beta$ for Tb^{III} ion and 3 $N\beta$ for Co^{II} ion) and 13 $N\beta$ (10 $N\beta$ for Dy^{III} ion and 3 $N\beta$ for Co^{II} ion), respectively, due to the crystal field effect on the Tb^{III} and Dy^{III} ions.

Magnetic Interaction between Cu^{II} and Ln^{III} Ions. Due to the orbital contribution of the Ln^{III} component, it is difficult to theoretically simulate the magnetic properties of the Cu^{II}–Tb^{III} and Cu^{II}–Dy^{III} complexes. The nature of the magnetic interaction between Cu^{II} and Ln^{III} ions were investigated by an empirical approach[27,28] based on a comparison of the magnetic susceptibilities of Cu^{II}–Ln^{III} with those of the isostructural Zn^{II}–Ln^{III} complexes involving the diamagnetic Zn^{II} ion. According to this approach, defining $\Delta(T) = (\chi_M T)_{CuLn} - (\chi_M T)_{ZnLn}$, we can write the following equation: $\Delta(T) = [(\chi_M T)_{Cu} + (\chi_M T)_{Ln} + J_{CuLn}(T)] - [(\chi_M T)_{Zn} + (\chi_M T)_{Ln}] = (\chi_M T)_{Cu} + J_{CuLn}(T)$, where $(\chi_M T)_{Zn}$ is diamagnetic and $(\chi_M T)_{Cu}$ represents the $\chi_M T$ value imputable to an isolated Cu^{II} ion (Curie constant: $(\chi_M T)_{Cu} = 0.375$ cm^3 K mol^{-1}) and the temperature-dependent contribution $J_{CuLn}(T)$ is related to the nature of the overall exchange interactions between the Cu^{II} and Ln^{III} ions. It should be noted that in general the M^{II}–Ln^{III} magnetic interaction $J_{MLn}(T)$ is weak and the pronounced $\Delta(T)$ value appears at the lower temperature region. The plots of $\Delta(T)$ versus T are given in Figure 7a. The above equation gives the relation of $J_{CuLn}(T) = \Delta(T) - (\chi_M T)_{Cu}$. When the $\Delta(T)$ value is larger than $(\chi_M T)_{Cu} = 0.375$ cm^3 K mol^{-1}, $J_{CuLn}(T)$ is positive, and consequently the magnetic interaction between Cu^{II} and Ln^{III} ions is ferromagnetic, while when the $\Delta(T)$ value is smaller than 0.375 cm^3 K mol^{-1}, $J_{CuLn}(T)$ is negative and indicates antiferromagnetic Cu^{II}–Ln^{III} interactions. The $\Delta(T)$ value for the Cu^{II}–Gd^{III} complex is larger than 0.375 cm^3 K mol^{-1} over the entire temperature region and increases on lowering the temperature, indicating a ferromagnetic interaction, in agreement with the quantitative fitting in terms of the isotropic spin Hamiltonian described above.

The $\Delta(T)$ values for the Cu^{II}–Tb^{III} complex are constant and slightly below 0.375 cm^3 K mol^{-1} in the temperature region 35–300 K and then increase to values above 0.375 cm^3 K mol^{-1} reaching a maximum around 10 K to finally decrease abruptly to a negative value. The $\Delta(T)$ values for the Cu^{II}–Dy^{III} complex are constant and slightly below 0.375 cm^3 K mol^{-1} in the temperature region 80–300 K and monotonically increase above 0.375 cm^3 K mol^{-1} on decreasing the temperature.

While for the Cu^{II}–Dy^{III} complex the monotonical increase of $\Delta(T)$ at low temperaures indicates a ferromagnetic Cu^{II}–Dy^{III}, the $\Delta(T)$ versus T plot for the Cu^{II}–Tb^{III} complex does not give a clear answer about the nature of the Cu^{II}–Tb^{III} magnetic interaction. The failure of the present empirical approach for the Cu^{II}–Tb^{III} complex is quite unexpected since the compared Cu^{II}–Tb^{III} and Zn^{II}–Tb^{III} complexes have an isomorphous structure. A possible explanation for the low temperature decrease of $\Delta(T)$ may be the occurrence of weak intermolecular antiferromagnetic interaction, for the Cu^{II}–Tb^{III} than for the Zn^{II}–Tb^{III} complex. Another possible explanation of this behavior could be a higher crystal field splitting experienced by the Tb^{III} ion in the Cu^{II}–Tb^{III} than in the Zn^{II}–Tb^{III} complex so that, at low temperatures, the $(\chi_M T)_{Tb}$ contribution in Cu^{II}–Tb^{III} is lower than that in Zn^{II}–Tb^{III} and their difference overcomes the small interaction term $J_{CuLn}(T)$. This effect is probably related to the larger size of the Zn^{II} than the Cu^{II} ion, see Table 2, leading to a significant variation of the coordination sphere around the Ln^{III} ion when passing from the Zn^{II}–Ln^{III} to the Cu^{II}–Ln^{III} complex, and is observed only for the Cu^{II}–Tb^{III} complex for which the interaction term $J_{CuLn}(T)$ is smaller. However, the increase of $\Delta(T)$ in the temperature range 50–10 K suggests an overall ferromagnetic Cu^{II}–Tb^{III} interaction.

dx.doi.org/10.1021/ic400594u | Inorg. Chem. 2013, 52, 6160–6178

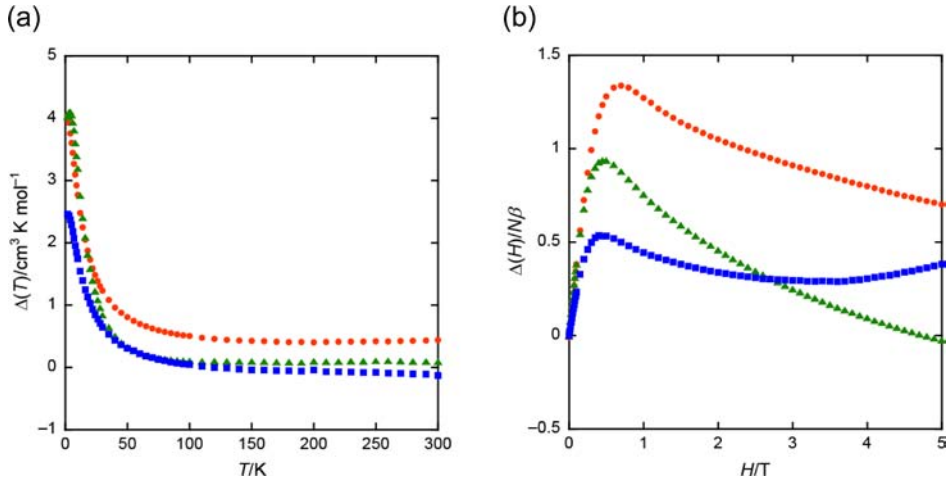

Figure 8. (a) Plots of $\Delta\chi_M(T) = (\chi_M T)_{NiLn} - (\chi_M T)_{ZnLn} - (\chi_M T)_{NiLa}$ vs T for the Ni^{II}–Ln^{III} complexes [Ln^{III} = Gd^{III} (red), Tb^{III} (green), and Dy^{III} (blue)]. (b) Plots of $\Delta(H) = M_{NiLn}(H) - M_{ZnLn}(H) - M_{NiLa}(H)$ vs H for the Ni^{II}–Ln^{III} complexes [Ln^{III} = Gd^{III} (red), Tb^{III} (green), and Dy^{III} (blue)].

Although not investigated by this empirical approach, ferromagnetic Cu^{II}–Ln^{III} interactions, (Ln^{III} = Gd^{III}, Dy^{III}, Tb^{III}) have been reported for dinuclear [$Cu^{II}Ln^{III}$] complexes by Costes et al.,[28a,b] 2D ladder-type [$Ln^{III}_2Cu^{II}_3$] complexes by Kahn et al.,[29] and trinuclear complexes Cu^{II}–Ln^{III}–Cu^{II} complexes $[Ln^{III}L_2(NO_3)_2\{Cu^{II}(CH_3OH)\}_2](NO_3)(CH_3OH)$ (L = 2,6-bis(acetylacetonato)pyridine) by Ishida et al.[30] and Okawa et al.[31] An overview of the plots of $\Delta(T)$ versus T of Figure 7a shows that the plot for the Cu^{II}–Gd^{III} complex lies on the top, that for the Cu^{II}–Dy^{III} complex in the middle, and that for the Cu^{II}–Tb^{III} complex on the bottom, indicating the $J_{CuLn}(T)$ is in the order $J_{CuGd}(T) > J_{CuDy}(T) > J_{CuTb}(T)$. This trend slightly differs from the results by Ishida et al.,[30] who studied the ferromagnetic exchange coupling of Cu^{II}–Ln^{III}–Cu^{II} complexes $[Ln^{III}L_2(NO_3)_2\{Cu^{II}(CH_3OH)\}_2](NO_3)(CH_3OH)$ by high-frequency electron paramagnetic resonance and magnetization studies and revealed that the exchange coupling J(Cu–Ln) was in the order J(Cu–Gd) > J(Cu–Tb) > J(Cu–Dy).

The same empirical approach was applied to the magnetization curves at constant temperature and gives complementary information on the magnetic interaction between Cu^{II} and Ln^{III} ions at the lowest considered temperature of 1.9 K. Let us now define $\Delta(H) = M_{CuLn}(H) - M_{ZnLn}(H) = [M_{Cu}(H) + M_{Ln}(H) + J_{CuLn}(H)] - [M_{Zn}(H) + M_{Ln}(H)] = M_{Cu}(H) + J_{CuLn}(H)$, where M is the magnetization measured on the complex denoted by the subscript and the magnetization of the diamagnetic Zn^{II} component $M_{Zn}(H)$ and the contribution from the Zn^{II}–Ln^{III} interaction should be zero. This can be written as $\Delta(H) = M_{Cu}(H) + J_{CuLn}(H)$, where $M_{Cu}(H)$ is the magnetization for an independent Cu^{II} ion, that can be calculated by the corresponding Brillouin function, while the extra contribution $J_{CuLn}(H)$ is related to the nature of the overall exchange magnetic interactions between the Cu^{II} and Ln^{III} ions. As the quantity $(\Delta(H) - M_{Cu}(H))$ represents the deviation from the limit situation in which Cu^{II} and Ln^{III} ions are magnetically independent, positive values of $J_{CuLn}(H)$, i.e., $\Delta(H)$ lying above M_{Cu}(H), indicate ferromagnetic Cu^{II}–Ln^{III} interactions while negative values of $J_{CuLn}(H)$, i.e., $\Delta(H)$ lying below $M_{Cu}(H)$, indicate antiferromagnetic Cu^{II}–Ln^{III} interactions. The values of the parameter $\Delta(H)$ are plotted in Figure 7b as a function of the field and compared with the Brillouin function for one independent Cu^{II} ion. The $\Delta(H)$ versus H plot for the Cu^{II}–Gd^{III} complex lies well above $M_{Cu}(H)$ in the whole range of H, thus confirming the ferromagnetic nature of the interaction between Cu^{II} and Gd^{III} ions. Also the $\Delta(H)$ versus H plot for the Cu^{II}–Dy^{III} complex lies above $M_{Cu}(H)$, although slightly lower at high applied field, indicating again a ferromagnetic Cu^{II}–Dy^{III} interaction. On the other hand, the $\Delta(H)$ versus H plot for the Cu^{II}–Tb^{III} complex lies below $M_{Cu}(H)$ at low magnetic field and above $M_{Cu}(H)$ at magnetic field above 1 T: the behavior at low field is probably due to larger intermolecular interactions or a higher crystal field splitting experienced by the Tb^{III} ion in the Cu^{II}–Tb^{III} than in the Zn^{II}–Tb^{III} complex (see discussion above) whose effect is maximum at the lowest considered temperature of 1.9 K. However, the increase at higher field confirms that also the Cu^{II}–Tb^{III} interaction is ferromagnetic. The result from the field dependent magnetization measurements is consistent with the result from the temperature-dependent magnetic susceptibility measurements, taking into account that the $\Delta(T)$ and $\Delta(H)$ values are not always above the reference Cu curves over whole regions of T and H. The detailed explanation for the anomalous $\Delta(T)$ and $\Delta(H)$ behaviors is left to a further study.

Magnetic Interaction between Ni^{II} and Ln^{III} Ions. Since the magnetic properties of the Ni^{II}–Ln^{III} complexes involve important orbital contributions from the Ni^{II} and Ln^{III} ions, the nature of the magnetic interaction between Ni^{II} and the 4f magnetic ions was investigated by the same empirical approach employed above.[22,23] Now the Ni^{II}–Ln^{III} complexes involve an orbital contribution from the Ni^{II} ion too, and therefore, we have included also $\chi_M T$ values of Ni^{II}–La^{III} complex in the empirical approach. The difference between the $\chi_M T$ values for the Ni^{II}–Ln^{III}, Zn^{II}–Ln^{III}, and Ni^{II}–La^{III} complexes, $\Delta(T) = (\chi_M T)_{NiLn} - (\chi_M T)_{ZnLn} - (\chi_M T)_{NiLa} = [(\chi_M T)_{Ni} + (\chi_M T)_{Ln} + J_{NiLn}(T)] - [(\chi_M T)_{Zn} + (\chi_M T)_{Ln}] - [(\chi_M T)_{Ni} + (\chi_M T)_{La}] = J_{NiLn}(T)$, where the terms $(\chi_M T)_{Zn}$ and $(\chi_M T)_{La}$ referring to diamagnetic species are zero and the temperature-dependent contribution $J_{NiLn}(T)$ is related to the nature of the overall exchange interactions between the Ni^{II} and Ln^{III} ions. Since the Ni^{II}–Ln^{III} magnetic interaction $J_{NiLn}(T)$ is weak, a positive or a negative value of the $\Delta(T)$ in the lower temperature region is directly related to a ferro- or antiferromagnetic interaction, respectively. Figure 8a reports the values of $\Delta(T)$ versus T for the Ni^{II}–Gd^{III}, Ni^{II}–Tb^{III}, and Ni^{II}–Dy^{III} complexes. Since $J_{NiLn}(T) = \Delta(T)$, when $\Delta(T)$ and then $J_{NiLn}(T)$ is positive, the magnetic interactions between Ni^{II} and

dx.doi.org/10.1021/ic400594u | Inorg. Chem. 2013, 52, 6160–6178

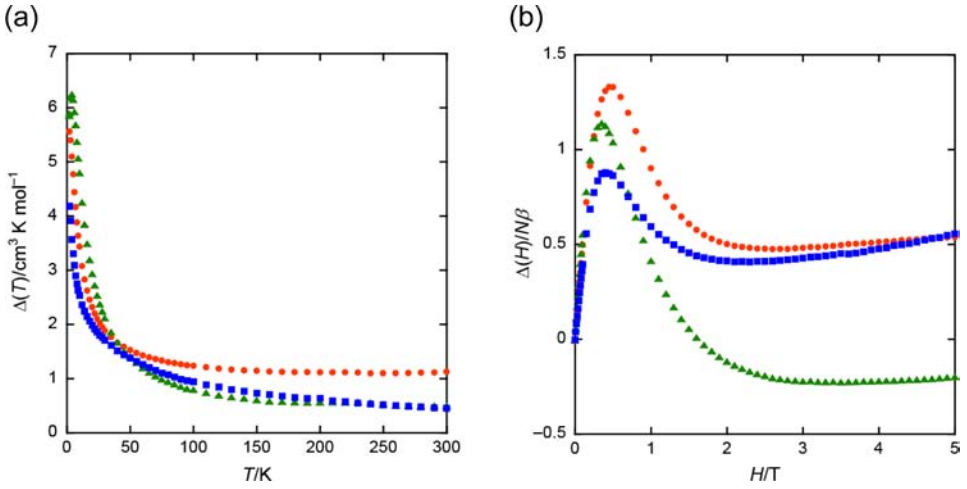

Figure 9. (a) Plots of $\Delta(T) = (\chi_M T)_{CoLn} - (\chi_M T)_{CoLa} - (\chi_M T)_{ZnLn}$ vs temperature T for the Co^{II}–Ln^{III} complexes [Ln^{III} = Gd^{III} (red), Tb^{III} (green), and Dy^{III} (blue)]. (b) Plots of $\Delta(H) = M_{CoLn}(H) - M_{CoLa}(H) - M_{ZnLn}(H)$ vs H for the Co^{II}–Ln^{III} complexes [Ln^{III} = Gd^{III} (red), Tb^{III} (green), and Dy^{III} (blue)].

Ln^{III} ions are ferromagnetic, while negative values of $\Delta(T)$ and then of $J_{NiLn}(T)$ indicate antiferromagnetic Ni^{II}–Ln^{III} interactions. As shown in Figure 8a, the $\Delta(T)$ values for Ni^{II}–Gd^{III} and Ni^{II}–Tb^{III} complexes are positive in the whole temperature range 1.9–300 K and show a marked increase below 100 K, while those for Ni^{II}–Dy^{III} complex are slightly negative at room temperature but become positive on lowering the temperature, also showing a marked increase below 100 K. This empirical approach thus shows for all three Ni^{II}–Gd^{III}, Ni^{II}–Tb^{III}, and Ni^{II}–Dy^{III} complexes an intramolecular d–f ferromagnetic interaction.

The same empirical approach was applied to the magnetization values at constant temperature and gives complementary information on the magnetic interaction between Ni^{II} and Ln^{III} ions. Let us now define $\Delta(H) = M_{NiLn}(H) - M_{ZnLn}(H) - M_{NiLa}(H) = [M_{Ni}(H) + M_{Ln}(H) + J_{NiLn}(H)] - [M_{Zn}(H) + M_{La}(H)] - [M_{Ni}(H) + M_{La}(H)]$, where M is the magnetization measured on the complex denoted by the subscript. The terms of $M_{Zn}(H)$ and $M_{La}(H)$ consisting of diamagnetic species should be zero. This parameter can be written as $\Delta(H) = J_{NiLn}(H)$, where $J_{NiLn}(H)$ is related to the nature of the overall exchange magnetic interactions between the Ni^{II} and Ln^{III} ions. As the quantity $\Delta(H)$ represents the deviation from the limit situation in which Ni^{II} and Ln^{III} ions are magnetically independent, positive values of $J_{NiLn}(H)$ indicate ferromagnetic Ni^{II}–Ln^{III} interactions while negative values of $J_{NiLn}(H)$ indicate antiferromagnetic Ni^{II}–Ln^{III} interactions.

The values of the parameter $\Delta(H)$ are plotted in Figure 8b as the function of the magnetic field. The $\Delta(H)$ versus H plots for the all three Ni^{II}–Ln^{III} complexes lie well above zero in the whole range of H, thus suggesting the ferromagnetic nature of the interaction between Ni^{II} and Ln^{III} ions for all three Ni^{II}–Gd^{III}, Ni^{II}–Tb^{III}, and Ni^{II}–Dy^{III} complexes. The ferromagnetic feature derived from the magnetization measurements is thus consistent with the result from the magnetic susceptibility measurements. Regarding the peculiar $\Delta(H)$ profiles, showing a maximum around 0.4–0.7 T, the detailed explanation is left to a further study.

Overall, both $\Delta(T)$ versus T and $\Delta(H)$ versus H plots in Figure 8 show that the plot for the Ni^{II}–Gd^{III} complex lies close (on the top at high temperatures and fields) to that for the Ni^{II}–Tb^{III} complex and that for the Ni^{II}–Dy^{III} complex on the bottom, indicating that the ferromagnetic Ni^{II}–Ln^{III} interactions are in the order $J_{NiGd} \geq J_{NiTb} > J_{NiDy}$, with an inversion of the order for the Ni^{II}–Tb^{III} and Ni^{II}–Dy^{III} interactions with respect to that of the Cu^{II}–Tb^{III} and Cu^{II}–Dy^{III} interactions, see discussion above. This result slightly differs from the results by Pasatoiu et al.,[20b] who studied the ferromagnetic exchange coupling of closely related binuclear Ni^{II}–Ln^{III} complexes, $[Ni^{II}(CH_3CN)(H_2O)(3\text{-MeOsaltn})Ln^{III}(NO_3)_3(H_2O)_3]$, with the same tetradentate ligand for Ni^{II} ion but, different from our compounds, without an acetate ligand bridging Ni^{II} and Ln^{III} ions, finding that the exchange coupling $J_{Ni\text{-}Ln}$ was in the order $J_{NiDy} > J_{NiTb}$. This different behavior indicates that the magnetic Ni^{II}–Ln^{III} interactions are sensible to small changes of the number and the nature of bridging ligands. In addition to the existence or absence of a bridging acetato, the notable structural difference is seen in that the bridging core of $Ni^{II}O_2Ln^{III}$ is almost planar for the Ni^{II}–Ln^{III} complexes by Pasatoiu et al., while the dihedral angle between $Ni^{II}O_2$ and O_2Ln^{III} is 13.1° for the present complexes.

Magnetic Interaction between Co^{II} and Ln^{III} Ions. Since the magnetic properties of the Co^{II}–Ln^{III} complexes involve orbital contributions from both Co^{II} and Ln^{III} ions, the nature of the magnetic interaction between Co^{II} and the 4f magnetic ions was investigated by the same empirical approach for Ni^{II}–Ln^{III} complexes. The difference between the $\chi_M T$ values for the Co^{II}–Ln^{III}, Zn^{II}–Ln^{III}, and Co^{II}–La^{III} complexes is $\Delta(T) = (\chi_M T)_{CoLn} - (\chi_M T)_{ZnLn} - (\chi_M T)_{CoLa} = J_{CoLn}(T)$, where the temperature-dependent contribution $J_{CoLn}(T)$ is related to the nature of the overall exchange interactions between the Co^{II} and Ln^{III} ions. Figure 9a reports the values of $\Delta(T)$ versus T for the Co^{II}–Gd^{III}, Co^{II}–Tb^{III}, and Co^{II}–Dy^{III} complexes. Since $J_{CoLn}(T) = \Delta(T)$, when $\Delta(T)$ and then $J_{CoLn}(T)$ is positive, the magnetic interactions between Co^{II} and Ln^{III} ions are ferromagnetic, while negative values of $\Delta(T)$ and then of $J_{CoLn}(T)$ indicate antiferromagnetic Co^{II}–Ln^{III} interactions. The $\Delta(T)$ values for all the Co^{II}–Ln^{III} complexes are positive in the whole temperature range 1.9–300 K and increase abruptly on lowering the temperature, indicating a ferromagnetic interaction. This empirical approach applied to the magnetic susceptibilities thus indicates ferromagnetic interactions for all three Co^{II}–Ln^{III} complexes.

The same empirical approach was applied to the magnetization values at the constant temperature of 1.9 K and gives complementary information on the magnetic interaction between

dx.doi.org/10.1021/ic400594u | Inorg. Chem. 2013, 52, 6160–6178

Co^{II} and Ln^{III} ions. Let us now define $\Delta(H) = M_{CoLn}(H) - M_{ZnLn}(H) - M_{CoLa}(H)$, where M is the magnetization measured on the complex denoted by the subscript. This parameter can be written as $\Delta(H) = J_{CoLn}(H)$, where $J_{CoLn}(H)$ is related to the nature of the overall exchange magnetic interactions between the Co^{II} and Ln^{III} ions. As the quantity $\Delta(H)$ represents the deviation from the limit situation in which Co^{II} and Ln^{III} ions are magnetically independent, positive values of $J_{CoLn}(H)$ indicate ferromagnetic Co^{II}–Ln^{III} interactions while negative values of $J_{CoLn}(H)$ indicate antiferromagnetic Co^{II}–Ln^{III} interactions. The values of the parameter $\Delta(H)$ are plotted in Figure 9b versus the magnetic field H. The $\Delta(H)$ versus H plots lie well above zero, in the whole range of H for the Co^{II}–Gd^{III} and Co^{II}–Dy^{III} complexes, assuming small negative values only at high field (above 1.5 T) for Co^{II}–Tb^{III}, thus confirming the ferromagnetic nature of the interaction between Co^{II} and Ln^{III} ions. Although the $\Delta(T)$ versus T and $\Delta(H)$ versus H plots in Figure 9 do not give a very clear picture when considered in the whole considered temperature and field ranges, at low temperatures and fields the plot for the Co^{II}–Gd^{III} complex lies close to that for the Ni^{II}–Tb^{III} complex (above at high temperatures) and that for the Co^{II}–Dy^{III} complex on the bottom, suggesting that the ferromagnetic Co^{II}–Ln^{III} interactions are in the order $J_{CoGd} \geq J_{CoTb} > J_{CoDy}$, roughly the same order found for the Ni^{II}–Ln^{III} interactions.

Alternating Current Magnetic Properties of Cu^{II}–Ln^{III} Complexes (Ln^{III} = Tb^{III} and Dy^{III}). The Cu^{II}–Ln^{III} complexes exhibiting ferromagnetic interactions have been examined by ac magnetic susceptibility measurements, since one of the characteristics of an SMM is the observation of an out-of-phase (χ_M'') ac susceptibility signal. The temperature dependent ac magnetic measurements were carried out in a 3.0 Oe field oscillating at the indicated frequencies (10–1000 Hz) and with a zero dc field, down to a minimum temperature of 1.8 K. The Cu^{II}–Gd^{III} shows no frequency dependence under the experimental conditions. Figure S3 shows the results of the ac magnetic susceptibility measurements for the Cu^{II}–Tb^{III} and Cu^{II}–Dy^{III} complexes, as plots of χ_M' and χ_M'' versus T in the 1.8–20 K temperature range. As seen in Figure S3, the Cu^{II}–Tb^{III} complex shows no frequency-dependent signals in the same temperature range, while the Cu^{II}–Dy^{III} complex shows a very small dependence at the very low temperature. To evaluate a possible SMM behavior for the present systems, we further investigated χ_M' and χ_M'' with a dc bias field of 1000 Oe. The dc bias was applied to reduce a possible quantum tunneling of the magnetization.[32] The ac amplitude was 5.0 Oe field and frequencies of 10–10 000 Hz down to a lowest temperature of 1.8 K. Figure 10a,b shows the results of the ac magnetic susceptibility measurements for the Cu^{II}–Tb^{III} and Cu^{II}–Dy^{III} complexes. The Cu^{II}–Tb^{III} complex shows only slightly frequency-dependent signals, and Cu^{II}–Dy^{III} complex shows a small dependence at the very low temperature; an indication of χ_M'' upsurge was then observed for the latter complex, but no peak appeared above 1.8 K. The Cu^{II}–Dy^{III} complex has higher frequency dependence than that of the Cu^{II}–Tb^{III} complex.

It has been known that the appearance of ac signals for Cu^{II}–Ln^{III} SMMs is affected not only by the intramolecular magnetic interaction but also by the symmetry of the ligand field. Kajiwara et al. reported a correlation between the symmetry of the ligand field and the magnetic anisotropy of Tb^{III}–Cu^{II} dinuclear systems. He studied two related Cu^{II}–Tb^{III} complexes, which were prepared by the reactions $[Tb^{III}Cu^{II}(o\text{-vanilate})_2(NO_3)_3]$ with either methoxypropylamine or ethoxyethylamine.[13] When

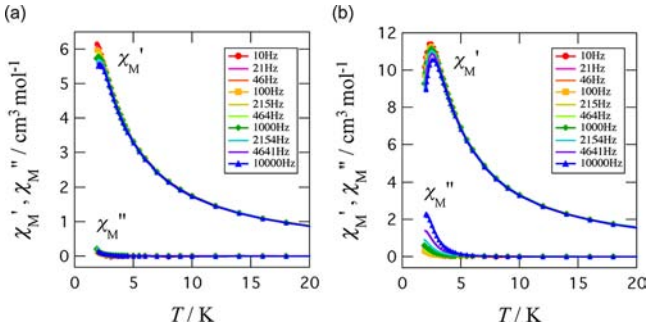

Figure 10. Plots of the in-phase (χ_M') and out-of-phase (χ_M'') ac susceptibilities as a function of temperature and frequency in the range 10–10 000 Hz, at H_{ac} = 5.0 Oe, and with a dc bias field of 1000 G for (a) the Cu^{II}–Tb^{III} complex, (b) the Cu^{II}–Dy^{III} complex.

the Tb^{III} ion is in a less symmetrical ligand field, it has an easy-axis anisotropy and shows SMM behavior, whereas when it is in a more symmetrical environment, it has an easy-plane anisotropy and exhibits non-SMM behavior. The present Cu^{II}–Tb^{III} and Cu^{II}–Dy^{III} complexes have a rather weaker ferromagnetic interaction between Cu^{II} and Ln^{III} ions and have a symmetrical ligand filed around Ln^{III} ion.

Alternating Current Magnetic Properties of Ni^{II}–Ln^{III} complexes (Ln^{III} = Gd^{III}, Tb^{III}, and Dy^{III}). The Ni^{II}–Ln^{III} complexes exhibiting ferromagnetic interactions have been examined by ac magnetic susceptibility measurements. Figure S4 shows the results of the ac magnetic susceptibility measurements in a 3.0 Oe field oscillating at the indicated frequencies (10–1000 Hz) and with a zero dc field for Ni^{II}–Gd^{III}, Ni^{II}–Tb^{III}, and Ni^{II}–Dy^{III} complexes, as plots of χ_M' and χ_M'', respectively. As seen in Figure S4, three Ni^{II}–Ln^{III} complexes show no frequency-dependent signals in the same temperature range, showing the absence of SMM behavior and demonstrating the influence of the 3d metal ion on the SMM behavior observed for the $Cu^{II}Ln^{III}$ which therefore is not the sole fact of the Tb^{III} or Dy^{III} centers. To evaluate a possible SMM behavior for the present systems, we further investigated χ_M' and χ_M'' with a dc bias field of 1000 Oe. Figure 11a–c shows the results of the ac magnetic susceptibility measurements for the Ni^{II}–Gd^{III}, Ni^{II}–Tb^{III}, and Ni^{II}–Dy^{III} complexes, respectively. The Ni^{II}–Gd^{III} complex shows practically no frequency-dependent signal, while the Ni^{II}–Dy^{III} complex shows a small dependence at the very low temperature. As for the Ni^{II}–Tb^{III} complex, notable frequency dependence emerged. The Ni^{II}–Tb^{III} complex has higher frequency dependence than that of the Ni^{II}–Dy^{III} complex. On cooling, an increase of χ_M'' was found together with a decrease of χ_M'. Cole–Cole plots and Arrhenius plots of Ni^{II}–Tb^{III} complex are shown in Figure 11d,e, respectively. When we plotted the χ_M'' against χ_M' at various temperatures according to the Cole–Cole analysis,[33] a semicircle was clearly drawn at each temperature. The α value is considerably small (α = 0.221(7) at 2 K) in the Debye model, $\chi(\omega) = \chi_S + (\chi_T - \chi_S)/(1 + (i\omega\tau)^{1-\alpha})$ where χ_T and χ_S are the isothermal and adiabatic susceptibilities, respectively.[34] This finding guarantees a single relaxation process for this complex. The Arrhenius plot[35] of the Ni^{II}–Tb^{III} complex shows a straight line for the χ_M'' peak, and the activation energy (Δ) for the magnetization reversal was estimated as Δ/k_B = 14.9(6) K with $\tau_0 = 2.1(5) \times 10^{-7}$ s, where τ_0 stands for the pre-exponential factor in the Arrhenius equation, $\ln(2\pi\nu) = -\ln(\tau_0) - \Delta/k_BT$. The linear Arrhenius behavior down to 2 K indicates that the relaxation takes place mainly via thermal activation and that the

dx.doi.org/10.1021/ic400594u | Inorg. Chem. 2013, 52, 6160–6178

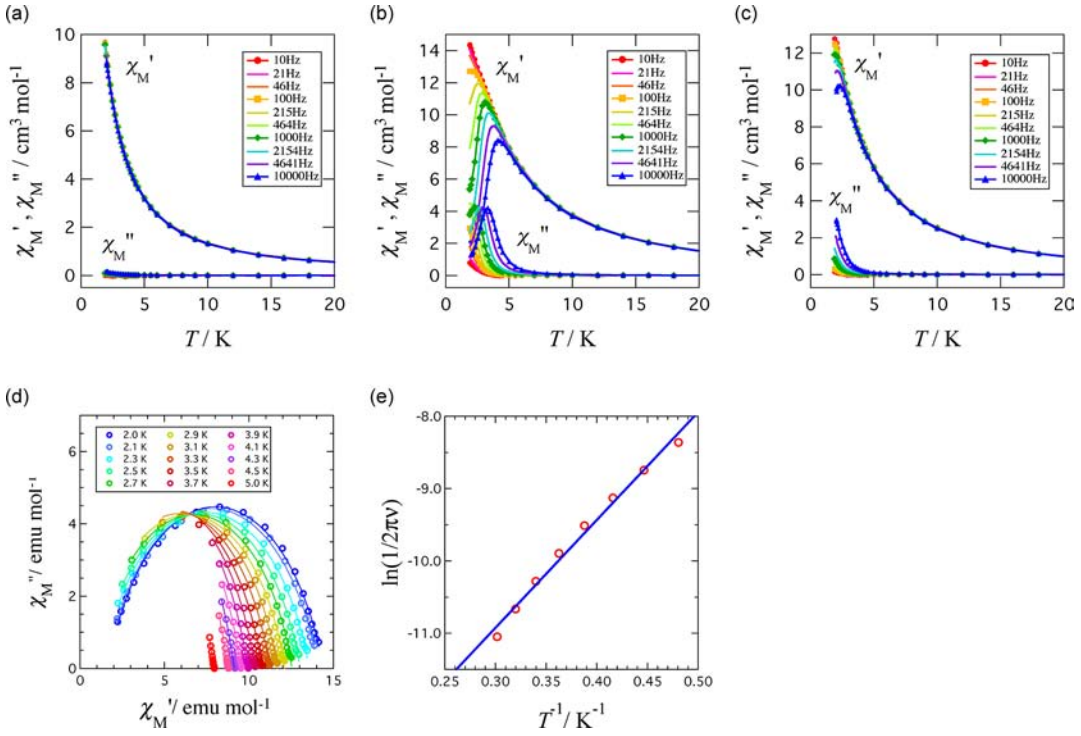

Figure 11. Plots of the in-phase (χ_M') and out-of-phase (χ_M'') ac susceptibility of (a) the Ni^{II}–Gd^{III}, (b) Ni^{II}–Tb^{III}, and (c) Ni^{II}–Dy^{III} complexes measured at a dc bias field of 1000 Oe, (d) Cole–Cole plot, and (e) Arrhenius plot of the Ni^{II}–Tb^{III} complex.

quantum tunneling of the magnetization is practically negligible at the 1000 Oe dc bias field. The present ac susceptibility behavior is typical of SMMs.

It is worth comparing the magnetic properties of our Ni^{II}–Ln^{III} complexes with those of similar binuclear Ni^{II}–Ln^{III} complexes. Pasatoiu et al. reported the structure and magnetic properties of the closely related binuclear Ni^{II}–Ln^{III} complexes, $[Ni^{II}(CH_3CN)(H_2O)(3\text{-MeOsaltn})Ln^{III}(NO_3)_3(H_2O)_3]$,[20b] with the same tetradentate ligand for Ni^{II} ion but, differently from our compounds, without an acetate ligand bridging Ni^{II} and Ln^{III} ions. Due to the acetato-bridging of Ni^{II} and Ln^{III} ions at their apical sites and at the same side, the Ni–O_2–Ln bridging core is more bent for our acetato-bridged compounds. While our Ni^{II}–Tb^{III} and Ni^{II}–Dy^{III} complexes show a pronounced and a slight frequency dependence of the ac susceptibilities under 1000 dc bias field, respectively, the [Ni^{II}–Tb^{III}] and [Ni^{II}–Dy^{III}] complexes of ref 20b show a slight and a moderate frequency dependence under the same conditions, respectively. Colacio et al. reported the structure and magnetic properties of acetato- or nitrato-bridged binuclear Ni^{II}–Dy^{III} complexes with *N,N′,N″*-trimethyl-*N,N″*-bis(2-hydroxy-3-methoxy-5-methylbenzyl)-diethylenetriamine, wherein for the nitrato-bridged complex a stronger ferromagnetic interaction between Ni^{II} and Dy^{III} ions is observed and an apparent frequency dependence of ac magnetic susceptibility is observed.[36] The difference in the magnetic properties between two complexes is ascribed to the planarity of Ni–O_2–Dy bridging core, in which the nitrato-bridged complex with a more planar Ni–O_2–Dy core gives a stronger ferromagnetic interaction between Ni^{II} and Dy^{III} ion and apparent frequency-dependent ac susceptibility. These data suggest that the acetate-bridging of the present Ni^{II}–Ln^{III} complexes gives a deviation from planar Ni–O_2–Dy bridging core to lead a different tendency of ferromagnetic interaction between Ni^{II} and Ln^{III} ions.[36]

Alternating Current Magnetic Properties of Co^{II}–Ln^{III} Complexes (Ln^{III} = Gd^{III}, Tb^{III}, and Dy^{III}). The Co^{II}–Ln^{III} complexes exhibiting ferromagnetic interactions have been examined by ac magnetic susceptibility measurements. Figure S5 shows the results of the ac magnetic susceptibility measurements for Co^{II}–Gd^{III}, Co^{II}–Tb^{III}, and Co^{II}–Dy^{III} complexes, as plots of χ_M' and χ_M''. As shown in Figure S5, Co^{II}–Gd^{III} and Co^{II}–Dy^{III} complexes show no frequency-dependent signals in the same temperature range. On the other hand, out-of-phase signal (χ_M'') of Co^{II}–Tb^{III} complex exhibits frequency-dependent behavior. This behavior is indicative of the slow relaxation of the magnetization, which is similar to those found for some lanthanide paramagnetic ions. Slow relaxation of the magnetization is directly responsible for behavior in SMM or SCM systems. Unfortunately, due to the 1.8 K temperature limit of the instrument, a maximum in the χ_M'' signal was not observed at frequencies as high as 1000 Hz. Slow relaxation of the magnetization is directly responsible for behavior in SMM systems.

We moved to study the SMM behavior with a dc bias field of 1000 Oe applied in this system. Figure 12a–c show the results of the ac magnetic susceptibility measurements for the Co^{II}–Gd^{III}, Co^{II}–Tb^{III}, and Co^{II}–Dy^{III} complexes, respectively. The Co^{II}–Gd^{III} complex shows practically no frequency-dependent signal, while the Co^{II}–Dy^{III} complex exhibits a small dependence at the very low temperature. Figure 12b displays the results on the Co^{II}–Tb^{III} complex, clarifying a drastic improvement of frequency dependence. The Co^{II}–Tb^{III} complex has higher frequency dependence than that of the Co^{II}–Dy^{III} complex. According to the Cole–Cole analysis, a semicircle was clearly drawn at each temperature. The α value is considerably small (α = 0.241(6) at 2 K), suggesting the presence of a single relaxation process for this complex. The Arrhenius plot of the Co^{II}–Tb^{III} complex (Figure 12e) afforded Δ/k_B = 17.0(4) K with τ_0 = $6.1(10) \times 10^{-8}$ s. The linear Arrhenius behavior down to 2 K indicates

dx.doi.org/10.1021/ic400594u | *Inorg. Chem.* 2013, 52, 6160–6178

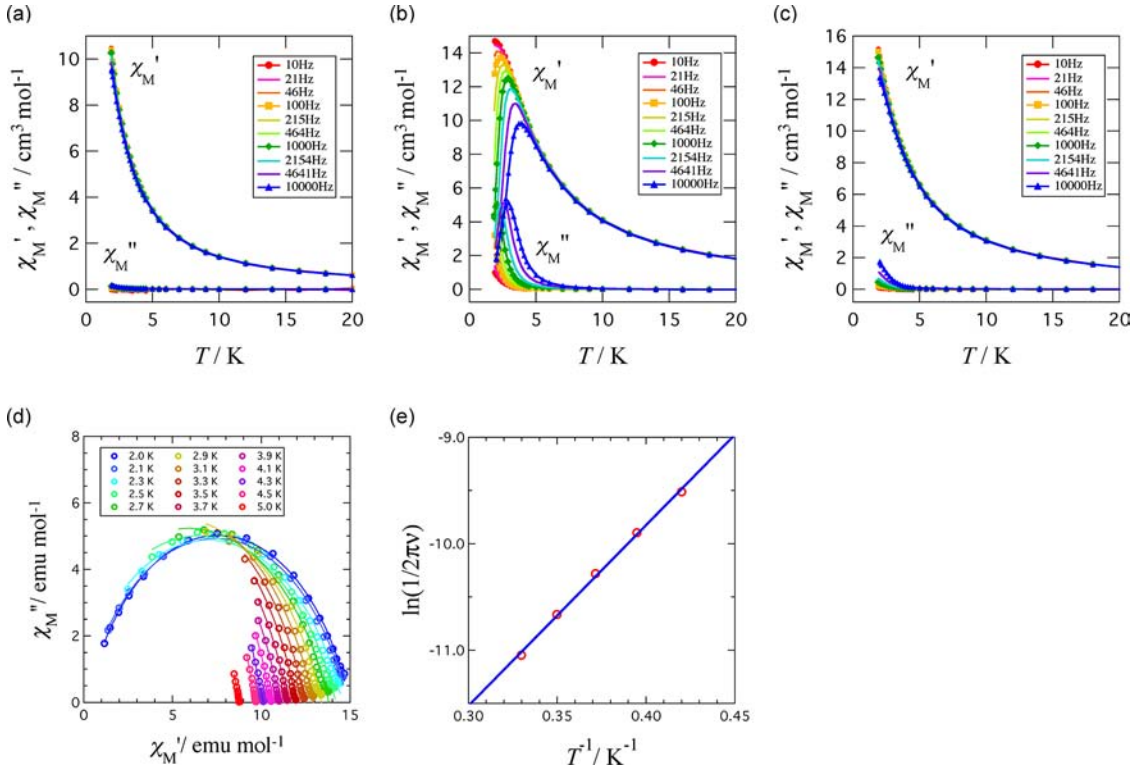

Figure 12. Plots of the in-phase (χ_M') and out-of-phase (χ_M'') ac susceptibility of (a) the Co^{II}–Gd^{III}, (b) Co^{II}–Tb^{III}, and (c) Co^{II}–Dy^{III} complexes measured at a dc bias field of 1000 Oe, (d) Cole–Cole plot, and (e) Arrhenius plot of the Co^{II}–Tb^{III} complex.

that the relaxation takes place mainly via thermal activation and that the quantum tunneling of the magnetization is practically negligible at the 1000 Oe dc bias field. From these ac susceptibility analyses, the Co^{II}–Tb^{III} complex is concluded to be an SMM.

Combining the results on the Ni^{II}–Ln^{III} and Co^{II}–Ln^{III} complexes, we can point out that a Tb^{III} ion is a more promising component candidate for SMMs than a Dy^{III} ion (Figures 11 and 12). On the other hand, the results on Cu^{II}–Ln^{III} complexes indicate that the Dy^{III} analogue has better characteristics than the Tb^{III} analogue (Figure 10). The measurement conditions including the magnitude of a bias field were not optimized, but a similar trend could be found from a closer look at the results without any dc field (Figure S3b), and the present difference is substantial. The Ni^{II}–Ln^{III} and Co^{II}–Ln^{III} complexes are isomorphous to each other but different from those of the Cu^{II}–Ln^{III} complexes, as the crystal structure analysis revealed. A plausible reason for this difference will be attributed to the structures around the Ln ions. Namely, the single-ion magnetic anisotropy and the exchange coupling are very sensitive to the Ln coordination structure, which regulates the SMM characteristics.

CONCLUSIONS

We have reported the series of acetato- and diphenolato-bridged 3d–4f heterometal binuclear complexes, $[M^{II}(3\text{-MeOsaltn})(MeOH)_x(ac)\,Ln^{III}(hfac)_2]$ (M^{II} = Co^{II}, Ni^{II}, Cu^{II}, Zn^{II}; Ln^{III} = Gd^{III}, Tb^{III}, Dy^{III}, and La^{III}) (x = 0 for M^{II} = Cu^{II}, Zn^{II}; x = 1 for M^{II} = Co^{II}, Ni^{II}), where 3-MeOsaltn and hfac denote *N*,*N*′-bis(3-methoxysalicyldene)-1,3-propanediaminato) and hexafluoroacetylacetonato, respectively. Magnetic interactions in these complexes were determined by removing the first-order orbital contributions of the M^{II} (M^{II} = Co^{II} or Ni^{II}) and Ln^{III} (Ln^{III} = Tb^{III} or Dy^{III}) ions using an empirical approach.[27,28] While some of the results are not simply indicative of the magnetic interaction, all these complexes suggested ferromagnetic interactions between M^{II} and Ln^{III} ions, in agreement with previous studies indicating that these types of Cu^{II}–Ln^{III} (Ln^{III} = Gd^{III}, Tb^{III}, and Dy^{III}) complexes usually showed ferromagnetic interaction. The magnitude of the ferromagnetic interaction, $J_{MLn}(T)$ and $J_{MLn}(H)$, are in the order Cu^{II}–Gd^{III} > Cu^{II}–Dy^{III} > Cu^{II}–Tb^{III}, while those are in the order of M^{II}–Gd^{III} ≈ M^{II}–Tb^{III} > M^{II}–Dy^{III} for M^{II} = Ni^{II} and Co^{II}. The alternating current magnetic measurement revealed that the Ni^{II}–Gd^{III} and Co^{II}–Gd^{III} complexes show practically no frequency-dependent signal, the Ni^{II}–Dy^{III} and Co^{II}–Dy^{III} complexes show a small dependence at the very low temperature, and the Ni^{II}–Tb^{III} and Co^{II}–Tb^{III} complexes show notable frequency dependence. The behavior of the frequency dependence in ac measurements may be related to the result of the magnetic interaction $J_{NiTb} > J_{NiDy}$ and $J_{CoTb} > J_{CoDy}$ from the temperature and field dependent magnetic measurements. The alternating current magnetic measurement revealed that the Ni^{II}–Tb^{III} and Co^{II}–Tb^{III} complexes could be attractive candidates for SMM behavior. From the Arrhenius analysis the energy barrier for the spin flipping was characterized to be 14.9(6) and 17.0(4) K for Ni^{II}–Tb^{III} and Co^{II}–Tb^{III}, respectively, under a dc bias field of 1000 Oe. Such a behavior would clearly originate from the anisotropic properties of both Ni^{II} or Co^{II} and Tb^{III} ions and their ferromagnetic exchange coupling. This observation suggests a possible way to pursue new 3d–4f SMM complexes by increasing the spin state and magnetic anisotropy through the use of anisotropic d metal ions, like Ni^{II} and Co^{II}. The present complexes do show ac signals at low temperature and would give effective information for the design of d–f SMMs.

dx.doi.org/10.1021/ic400594u | *Inorg. Chem.* 2013, 52, 6160–6178

EXPERIMENTAL SECTION

Materials. All reagents and solvents, obtained from Tokyo Kasei Co. and Wako Pure Chemical Industries, in the syntheses were of reagent grade, and they were used without further purification. The tetradentae Schiff-base ligand *N,N′*-bis(3-methoxy-2-oxybenzylidene)-1,3-propanediamine), abbreviated as $H_2$3-MeOsaltn, was obtained as yellow crystals by mixing 3-methoxysalicylaldehyde and 1,3-diaminopropane in a 2:1 mol ratio in methanol. The ligand was identified by the ^{1}H NMR spectrum and mp = 93 °C. The d-component complexes [M(3-MeOsaltn)$(H_2O)_x$] (M = Co^{II}, Ni^{II}, Cu^{II}, and Zn^{II}) were synthesized by mixing metal(II) acetate hydrate and H_2(3-MeOsaltn) in a 1:1 mol ratio in methanol, according to the literature applied for the M(salen) complexes,[37] in which the synthesis of [Co(3-MeOsaltn)$(H_2O)_2$] was carried out under a nitrogen atmosphere in order to avoid the air oxidation. Recrystallization was performed from chloroform.

[Gd(ac)(Hhfac)(hfac)$_2$(H_2O)$_2$]. To a solution of gadolinium acetate tetrahydrate $Gd^{III}(ac)_3{\cdot}4H_2O$ (0.406 g, 1 mmol) in 50 mL of water was added Hhfac (hexafluoroacetylacetone) (0.618 g, 3 mmol) in small amount of methanol under stirring at room temperature in a hood. The mixture was stirred for 1 h, and the white precipitate was collected by filtration. The filtrate was recrystallized from diethyl ether. Colorless needle crystals. Anal. Calcd for $C_{17}H_{12}O_{10}F_{18}Gd$ = [Gd(ac)(Hhfac)-(hfac)$_2$(H_2O)$_2$]: C; 23.32, H; 1.38%. Found: C; 23.35, H; 1.27%. IR (KBr disk):1650, 1560, ν(C−F) 1255, 1209, 1143 cm^{-1}.

[Tb(ac)(Hhfac)(hfac)$_2$(H_2O)(MeOH)]. The complex was prepared by a similar method for [Gd^{III}(ac)(Hhfac)(hfac)$_2$(H_2O)$_2$]. Colorless needle crystals. Anal. Calcd for $C_{17}H_7O_8F_{18}Tb{\cdot}H_2O{\cdot}MeOH$ = [Tb(ac)-(Hhfac)(hfac)$_2$(H_2O)(MeOH)]: C; 24.28, H; 1.47%. Found: C; 24.38, H; 1.45%. IR (KBr disk):1650, 1564, ν(C−F) 1255, 1209, 1143 cm^{-1}.

[Dy(ac)(Hhfac)(hfac)$_2$(H_2O)(MeOH)]. The complex was prepared by a similar method for [Gd^{III}(ac)(Hhfac)(hfac)$_2$(H_2O)$_2$]. Colorless needle crystals. Anal. Calcd for $C_{17}H_7O_8F_{18}Dy{\cdot}H_2O{\cdot}MeOH$ = [Dy(ac)-(Hhfac)(hfac)$_2$(H_2O)(MeOH)]: C; 24.19, H; 1.47%. Found: C; 24.53, H; 1.34%. IR (KBr disk): 1650, 1560, ν(C−F) 1255, 1209, 1141 cm^{-1}.

[La(ac)(Hhfac)(hfac)$_2$(H_2O)$_2$]. Colorless needle crystals. Anal. Calcd for $C_{17}H_{12}O_{10}F_{18}La$ = [La(ac)(Hhfac)(hfac)$_2$(H_2O)$_2$]: C; 23.85, H; 1.30%. Found: C; 23.88, H; 1.45%.

[Cu(3-MeOsaltn)(ac)Gd(hfac)$_2$]. To a solution of [Gd(ac)(Hhfac)-(hfac)$_2$(H_2O)$_2$] (0.175 g, 0.2 mmol) in 20 mL of acetone was added a solution of [Cu(3-MeOsaltn)] (0.081 g, 0.2 mmol) in 20 mL of acetone at room temperature. The mixture was filtered, and the filtrate, clear green solution, was left at room temperature for several days to precipitate green plate crystals. They were collected by filtration and dried *in vacuo*. Yield: 0.139 g (67%). [Cu(3-MeOsaltn)(ac)Gd(hfac)$_2$], Anal. Calcd for $C_{31}H_{25}N_2O_{10}F_{12}CuGd$: C; 36.00, H; 2.44, N; 2.71%. Found: C; 36.00, H; 2.67, N; 2.84%. IR (KBr disk): ν(C═O) 1658; ν(C═N) 1623; ν_{asm}(CO) 1554; ν_{sym}(CO) 1442; ν(C−F) 1255, 1199, 1147 cm^{-1}.

[Cu(3-MeOsaltn)(ac)Tb(hfac)$_2$]. The complex was prepared by a similar method for [Cu(3-MeOsaltn)(ac)Gd(hfac)$_2$]. Green plate crystals. Yield: 0.131 g (63%). Anal. Calcd for $C_{31}H_{25}N_2O_{10}F_{12}CuTb$ = [Cu(3-MeOsaltn)(ac)Tb(hfac)$_2$]: C; 35.94, H; 2.43, N; 2.70%. Found: C; 35.83, H; 2.56, N; 2.88%. IR (KBr disk): ν(C═O) 1658; ν(C═N) 1623;ν_{asm}(CO) 1554; ν_{sym}(CO) 1442; ν(C−F) 1255, 1216, 1147 cm^{-1}.

[Cu(3-MeOsaltn)(ac)Dy(hfac)$_2$]. The complex was prepared by a similar method for [Cu(3-MeOsaltn)(ac)Gd(hfac)$_2$]. Green plate crystals. Yield: 0.141g (68%). Anal. Calcd for $C_{31}H_{25}N_2O_{10}F_{12}CuDy$ = [Cu(3-MeOsaltn)(ac)Dy(hfac)$_2$]: C; 35.82, H; 2.42, N; 2.69%. Found: C; 35.96, H; 2.52, N; 2.71%. IR (KBr disk): ν(C═O) 1658; ν(C═N) 1623;ν_{asm}(CO) 1554; ν_{sym}(CO) 1442; ν(C−F) 1255, 1216, 1147 cm^{-1}.

[Zn(3-MeOsaltn)(ac)Gd(hfac)$_2$]. A acetone solution of [Gd(ac)-(Hhfac)(hfac)$_2$(H_2O)$_2$] (0.175 g, 0.2 mmol) was added to a acetone solution of [Zn(3-MeOsaltn)] (0.081 g, 0.2 mmol). The solution was left at room temperature for several days to precipitate yellow plate crystals. They were collected by filtration and dried in *vacuo*. Yield: 0.120 g (58%). Anal. Calcd for $C_{31}H_{25}N_2O_{10}F_{12}ZnGd$ = [Zn(3-MeOsaltn)-(ac)Gd(hfac)$_2$]: C; 35.93, H; 2.43, N; 2.70%. Found: C; 36.25, H; 2.56, N; 2.85%. IR (KBr disk): ν(C═O) 1656; ν(C═N) 1625;ν_{asm}(CO) 1554; ν_{sym}(CO) 1442; ν(C−F) 1255, 1218, 1147 cm^{-1}.

[Zn(3-MeOsaltn)(ac)Tb(hfac)$_2$]. The complex was prepared by a similar method for [Zn(3-MeOsaltn)(ac)Gd(hfac)$_2$]. Yellow plate crystals. Yield: 0.129 g (62%). Anal. Calcd for $C_{31}H_{25}N_2O_{10}F_{12}ZnTb$ = [Zn(3-MeOsaltn)(ac)Tb(hfac)$_2$]: C; 35.88, H; 2.43, N; 2.70%. Found: C; 36.05, H; 2.54, N; 2.84%. IR (KBr disk): ν(C═O) 1658; ν(C═N) 1625;ν_{asm}(CO) 1554; ν_{sym}(CO) 1442; ν(C−F) 1257, 1218, 1147 cm^{-1}.

[Zn(3-MeOsaltn)(ac)Dy(hfac)$_2$]. The complex was prepared by a similar method for [Zn(3-MeOsaltn)(ac)Gd(hfac)$_2$]. Yellow plate crystals. Yield: 0.135 g (65%). Anal. Calcd for $C_{31}H_{25}N_2O_{10}F_{12}ZnDy$ = [Zn(3-MeOsaltn)(ac)Dy(hfac)$_2$]: C; 35.75, H; 2.42, N; 2.69%. Found: C; 35.85, H; 2.78, N; 2.71%. IR (KBr disk): ν(C═O) 1658; ν(C═N) 1639;ν_{asm}(CO) 1562; ν_{sym}(CO) 1440; ν(C−F) 1257, 1218, 1147 cm^{-1}.

[Ni(3-MeOsaltn)(MeOH)(ac)Gd(hfac)$_2$]. A mixed solution of acetone and methanol (1:1 by volume) of [Gd(ac)(Hhfac)(hfac)$_2$(H_2O)$_2$] (0.175 g, 0.2 mmol) was added to a mixed solution of acetone and methanol (1:1 by volume) of [Ni(3-MeOsaltn)] (0.080 g, 0.2 mmol). The solution was left at room temperature for several days to precipitate blue plate crystals. They were collected by filtration and dried in *vacuo*. The crystal solvent methanol was lost on drying. Yield: 0.117 g (54%). Anal. Calcd for $C_{32}H_{31}N_2O_{12}F_{12}NiGd$ = [Ni(3-MeOsaltn)(MeOH)-(ac)Gd(hfac)$_2$]·H_2O: C; 35.60, H; 2.89, N; 2.59%. Found: C; 35.69, H; 2.94, N; 2.76%. IR (KBr disk): ν(C═O) 1654; ν(C═N) 1633;ν_{asm}(CO) 1560; ν_{sym}(CO) 1440; ν(C−F) 1257, 1220, 1151 cm^{-1}.

[Ni(3-MeOsaltn)(MeOH)(ac)Tb(hfac)$_2$]. The complex was prepared by a almost similar method for [Ni(3-MeOsaltn)(MeOH)(ac)-Gd(hfac)$_2$]. Blue plate crystals. Yield: 0.123 g (57%). Anal. Calcd for $C_{32}H_{31}N_2O_{12}F_{12}NiTb$ = [Ni(3-MeOsaltn)(MeOH)(ac)Tb-(hfac)$_2$]·H_2O: C; 35.55, H; 2.89, N; 2.59%. Found: C; 35.61, H; 2.70, N; 2.85%. IR (KBr disk): ν(C═O) 1654; ν(C═N) 1633;ν_{asm}(CO) 1560; ν_{sym}(CO) 1440; ν(C−F) 1257, 1220, 1149 cm^{-1}.

[Ni(3-MeOsaltn)(MeOH)(ac)Dy(hfac)$_2$]. The complex was prepared by a almost similar method for [Ni(3-MeOsaltn)(MeOH)(ac)-Gd(hfac)$_2$]. Blue plate crystals. Yield: 0.121 g (56%). Anal. Calcd for $C_{32}H_{33}N_2O_{13}F_{12}NiDy$ = [Ni(3-MeOsaltn)(MeOH)(ac)Dy-(hfac)$_2$]·2H_2O: C; 34.85, H; 3.02, N; 2.54%. Found: C; 34.89, H; 2.83, N; 2.78%. IR (KBr disk): ν(C═O) 1654; ν(C═N) 1633;ν_{asm}(CO) 1560; ν_{sym}(CO) 1440; ν(C−F) 1257, 1220, 1151 cm^{-1}.

[Ni(3-MeOsaltn)(MeOH)(ac)La(hfac)$_2$]. The complex was prepared by a almost similar method for [Ni(3-MeOsaltn)(MeOH)(ac)-Gd(hfac)$_2$]. Blue plate crystals. Yield: 0.115 g (54%). Anal. Calcd for $C_{32}H_{31}N_2O_{12}F_{12}NiLa$ = [Ni(3-MeOsaltn)(MeOH)(ac)La-(hfac)$_2$]·H_2O: C; 36.22, H; 2.94, N; 2.64%. Found: C; 35.88, H; 3.00, N; 2.67%.

[Co(3-MeOsaltn)(MeOH)(ac)Gd(hfac)$_2$]. A mixed solution of acetone and methanol (1:1 by volume) of [Gd(ac)(Hhfac)(hfac)$_2$(H_2O)$_2$] (0.175 g, 0.2 mmol) was added to a mixed solution of acetone and methanol (1:1 by volume) of [Co^{II}(3-MeOsaltn)] (0.080 g, 0.2 mmol). The resulting solution was filtered, and the filtrate was left at room temperature for several days to precipitate orange plate crystals. They were collected by filtration and dried *in vacuo*. The crystal solvent methanol was lost on drying. Yield: 0.108 g (50%). Anal. Calcd for $C_{32}H_{31}N_2O_{12}F_{12}CoGd$ = [Co(3-MeOsaltn)(MeOH)(ac)Gd-(hfac)$_2$]·H_2O: C; 35.60, H; 2.89, N; 2.59%. Found: C; 35.54, H; 2.91, N; 2.82%. IR (KBr disk): ν(C═O) 1656; ν(C═N) 1629; ν_{asm}(CO) 1556; ν_{sym}(CO) 1440; ν(C−F) 1257, 1218, 1147 cm^{-1}.

[Co(3-MeOsaltn)(MeOH)(ac)Tb(hfac)$_2$]. The complex was prepared by a similar method for [Co(3-MeOsaltn)(MeOH)(ac)Gd-(hfac)$_2$]. Orange plate crystals. Yield: 0.110 g (51%). Anal. Calcd for $C_{32}H_{31}N_2O_{12}F_{12}CoTb$ = [Co^{II}(3-MeOsaltn)(MeOH)(ac)-Tb^{III}(hfac)$_2$]·H_2O: C; 35.54, H; 2.89, N; 2.59%. Found: C; 35.92, H; 2.71, N; 2.85%. IR (KBr disk): ν(C═O) 1656; ν(C═N) 1629;ν_{asm}(CO) 1556; ν_{sym}(CO) 1440; ν(C−F) 1255, 1211, 1147 cm^{-1}.

[Co(3-MeOsaltn)(MeOH)(ac)Dy(hfac)$_2$]. The complex was prepared by a similar method for [Co(3-MeOsaltn)(MeOH)(ac)Gd(hfac)$_2$]. Orange plate crystals. Yield: 0.111 g (51%). Anal. Calcd for $C_{32}H_{31}N_2O_{12}F_{12}CoDy$ = [Co(3-MeOsaltn)(MeOH)(ac)Dy-(hfac)$_2$]·H_2O: C; 35.42, H; 2.88, N; 2.58%. Found: C; 35.79, H; 2.88, N; 2.72%. IR (KBr disk): ν(C═O) 1656; ν(C═N) 1629; ν_{asm}(CO) 1556; ν_{sym}(CO) 1440; ν(C−F) 1255, 1216, 1147 cm^{-1}.

dx.doi.org/10.1021/ic400594u | *Inorg. Chem.* 2013, 52, 6160−6178

[Co(3-MeOsaltn)(MeOH)(ac)La(hfac)$_2$]. The complex was prepared by a similar method for [Co(3-MeOsaltn)(MeOH)(ac)Gd(hfac)$_2$]. Orange plate crystals. Yield: 0.101 g (48%). Anal. Calcd for $C_{32}H_{31}N_2O_{12}F_{12}CoLa$ = [Co(3-MeOsaltn)(MeOH)(ac)La(hfac)$_2$]·H_2O: C; 36.21, H; 2.94, N; 2.64%. Found: C; 36.08, H; 2.93, N; 2.77%.

Physical Measurements. Elemental analyses (C, H, N) were carried out at the Center for Instrumental Analysis of Kumamoto University. Infrared spectra were recorded at room temperature using a JEOL JIR-6500W spectrometer with samples in KBr disks. Thermogravimetric analyses were carried out on a TG/DTA6200 (SII Nano Technology Inc.) instrument at the 10 K min^{-1} heating rate using ca. 2 mg sample. Temperature-dependent magnetic susceptibilities in the temperature range 1.9−300 K under an external magnetic field of 0.1 T and field-dependent magnetization measurements in an applied magnetic field from 0 to 5 T at 1.9 K were measured with an MPMS XLS SQUID susceptometer (Quantum Design, Inc.). Some microcrystalline samples consisting of Tb^{III} and Dy^{III} ions showed apparent reorientation in the applied magnetic field of 0.5 T. All samples dispersed in liquid paraffin to avoid orientation in the field, and the results are given in the text. The calibrations were performed with palladium. Alternating current magnetic measurements were carried out at University of Wroclaw in a 3.0 G ac field oscillating over the range 10−1000 Hz and on a PPMS equipped with an ac/dc magnetic probe (Quantum Design, Inc.) at The University of Electro-Communications. Corrections for diamagnetism were applied using Pascal's constants.

X-ray Crystallography. X-ray data were collected on a Rigaku Rapid imaging plate diffractometer with graphite monochromated Mo Kα radiation (λ = 0.710 69 Å) at 150 or 100 K. All the crystals have a tendency of efflorescense, to decompose gradually. Each crystal was coated by epoxy resin quickly and mounted on a glass rod and measured at 150 or 100 K. An empirical absorption correction was applied. The data were also corrected for Lorentz and polarization effects. The crystal structures were determined and refined by direct method using the CrystalStructure crystallographic software package.[38] The X-ray diffraction analyses have problems in the explanation of the disorder at some of hfac ligands even at the low temperature. Hydrogen atoms were refined using the riding model. CCDC 829232−829243 contain the supplementary crystallographic data for 12 complexes. These data can be obtained free of charge via http://www.ccdc.cam.ac.uk/conts/retrieving.html, or from the Cambridge Crystallographic Data Centre, 12 Union Road, Cambridge CB2 1EZ, U.K.; fax (+44) 1223−336−033; or e-mail deposit@ccdc.cam.ac.uk.

■ ASSOCIATED CONTENT

Ⓢ Supporting Information

Additional figures and crystallographic data in CIF format. This material is available free of charge via the Internet at http://pubs.acs.org.

■ AUTHOR INFORMATION

Corresponding Author

*E-mail: naohide@aster.sci.kumamoto-u.ac.jp. Fax: +81-96-342-3390.

Notes

The authors declare no competing financial interest.

■ ACKNOWLEDGMENTS

K.N. and T.F. were supported by the Research Fellowship of the Japan Society for the Promotion of Science, KAKENHI 00248556 and 00248498.

■ REFERENCES

(1) (a) Sessoli, R.; Gatteschi, D.; Caneschi, A.; Novak, M. A. *Nature* **1993**, *365*, 141−143. (b) Gatteschi, D.; Caneschi, A.; Pardi, L.; Sessoli, R. *Science* **1994**, *265*, 1054−1058. (c) Sessoli, R.; Tsai, H. L.; Schake, A. R.; Wang, S.; Vincent, J. B.; Folting, K.; Gatteschi, D.; Christou, G.; Hendrickson, D. N. *J. Am. Chem. Soc.* **1993**, *115*, 1804−1816. (d) Thomas, L.; Lionti, F.; Ballou, R.; Gatteschi, D.; Sessoli, R.; Barbara, B. *Nature* **1996**, *383*, 145−147. (e) Cadiou, C.; Murrie, M.; Paulsen, C.; Villar, V.; Wernsdorfer, W.; Winpenny, W. E. P. *Chem. Commun.* **2001**, 2666−2667. (f) Shores, M. P.; Sokol, J. J.; Long, J. R. *J. Am. Chem. Soc.* **2002**, *124*, 2279−2292. (g) Boskovic, C.; Brechin, E. K.; Streib, W. E.; Folting, K.; Bollinger, J. C.; Hendrickson, D. N.; Christou, G. *J. Am. Chem. Soc.* **2002**, *124*, 3725−3736. (h) Ritter, S. *Chem. Eng. News* **2004**, *82*, 29−32. (i) Gatteschi, D.; Sessoli, R. *Angew. Chem., Int. Ed.* **2003**, *42*, 268−297. (j) Wernsdorfer, W.; Sessoli, R. *Science* **1999**, *284*, 133−135. (k) Aubin, S. M. J.; Sun, Z.; Pardi, L.; Krzystek, J.; Folting, K.; Brunel, L. C.; Rheingold, A. L.; Christou, G.; Hendrickson, D. N. *Inorg. Chem.* **1999**, *38*, 5329−5340.

(2) (a) Ishikawa, N.; Sugita, M.; Ishikawa, T.; Koshihara, S.; Kaizu, Y. *J. Am. Chem. Soc.* **2003**, *125*, 8694−8695. (b) Ishikawa, N.; Sugita, M.; Wernsdorfer, W. *J. Am. Chem. Soc.* **2005**, *127*, 3650−3651.

(3) (a) Bencini, C.; Benelli, A.; Caneschi, A.; Carlin, R. L.; Dei, A.; Gatteschi, D. *J. Am. Chem. Soc.* **1985**, *107*, 8128−8136. (b) Benelli, A.; Bencini, C.; Caneschi, A.; Dei, A.; Gatteschi, D. *Inorg. Chem.* **1986**, *25*, 572−575. (c) Benelli, A.; Caneschi, A.; Gatteschi, D.; Guillou, O.; Pardi, L. *Inorg. Chem.* **1990**, *29*, 1750−1755. (d) Matsumoto, N.; Sakamoto, M.; Tamaki, H.; Okawa, H.; Kida, S. *Chem. Lett.* **1990**, 853−854.

(4) (a) Osa, S.; Kido, T.; Matsumoto, N.; Re, N.; Pochaba, A.; Mronzinski, J. *J. Am. Chem. Soc.* **2004**, *126*, 420−423. (b) Kido, T.; Nagasato, S.; Sunatsuki, Y.; Matsumoto, N. *Chem. Commun.* **2000**, 2113−2114.

(5) Mishra, A.; Wernsdorfer, W.; Abboud, K. A.; Christou, G. *J. Am. Chem. Soc.* **2004**, *126*, 15648−15649.

(6) Zaleski, C. M.; Depperman, E. C.; Kampf, J. W.; Kirk, M. L.; Pecoraro, V. *Angew. Chem., Int. Ed.* **2004**, *43*, 3912−3914.

(7) (a) Costes, J. P.; Dahan, F.; Wernsdorfer, W. *Inorg. Chem.* **2006**, *45*, 5−7. (b) Hamamatsu, T.; Yabe, K.; Towatari, M.; Matsumoto, N.; Re, N.; Pochaba, A.; Mrozinski, J. *Bull. Chem. Soc. Jpn.* **2007**, *80*, 523−529. (c) Hamamatsu, T.; Yabe, K.; Towatari, M.; Osa, S.; Matsumoto, N.; Re, N.; Pochaba, A.; Mrozinski, J.; Gallani, J. L.; Barla, A.; Imperia, P.; Paulsen, C.; Kappler, J. P. *Inorg. Chem.* **2007**, *46*, 4458−4468.

(8) Sun, Y. Q.; Liang, M.; Dong, W.; Yang, G. M.; Liao, D. Z.; Jiang, Z. H.; Yan, S. P.; Cheng, P. *Eur. J. Inorg. Chem.* **2004**, *7*, 1514−1521.

(9) Aronica, C.; Pilet, G.; Chastanet, G.; Wernsdorfer, W.; Jacquot, J. F.; Luneau, D. *Angew. Chem., Int. Ed.* **2006**, *45*, 4659−4662.

(10) Ferbinteanu, M.; Kajiwara, T.; Choi, K. Y.; Nojiri, H.; Nakamoto, A.; Kojima, N.; Cimpoesu, F.; Fujimura, Y.; Takaishi, S.; Yamashita, M. *J. Am. Chem. Soc.* **2006**, *128*, 9008−9009.

(11) Yamaguchi, T.; Sunatsuki, Y.; Ishida, H.; Kojima, M.; Akashi, H.; Re, N.; Matsumoto, N.; Pochaba, A.; Mrozinski, J. *Inorg. Chem.* **2008**, *47*, 5736−5745.

(12) Liu, J.-L.; Guo, F.-S.; Meng, Z.-S.; Zheng, Y.-Z.; Leng, J.-D.; Tong, M.-L.; Ungur, L.; Chibotaru, L. F.; Heroux, K. J.; Hendrickson, D. N. *Chem. Sci.* **2011**, *2*, 1268−1272.

(13) (a) Kajiwara, T.; Nakano, M.; Takaishi, S.; Yamashita, M. *Inorg. Chem.* **2008**, *47*, 8604−8606. (b) Kajiwara, T.; Nakano, M.; Takahashi, K.; Takaishi, S.; Yamashita, M. *Chem.—Eur. J.* **2011**, *17*, 196−205.

(14) (a) Chandrasekhar, V.; Pandian, B. M.; Azhakar, R.; Vittal, J. J.; Clérac, R. J. *Inorg. Chem.* **2007**, *46*, 5140−5142. (b) Yamaguchi, T.; Costes, J.-P.; Kishima, Y.; Kojima, M.; Sunatsuki, Y.; Bruefuel, N.; Tuchagues, J.-P.; Vendier, L.; Wernsdorfer, W. *Inorg. Chem.* **2010**, *49*, 9125−9135. (c) Costes, J.-P.; Vendier, L.; Wernsdorfer, W. *Dalton Trans.* **2011**, *40*, 1700−1706.

(15) (a) Sutter, J.-P.; Dhers, S.; Rajamani, R.; Ramasesha, S.; Costes, J.-P.; Duhayon, C.; Vendier, L. *Inorg. Chem.* **2009**, *48*, 5820−5828. (b) Long, J.; Chamoreau, L.-M.; Marvaud, V. *Dalton Trans.* **2010**, *39*, 2188−2190. (c) Mori, F.; Nyui, T.; Ishida, T.; Nogami, T.; Choi, K.-Y.; Nojiri, H. *J. Am. Chem. Soc.* **2006**, *128*, 1440−1441. (d) Ueki, S.; Ishida, T.; Nogami, T.; Choi, K.-Y.; Nojiri, H. *Chem. Phys. Lett.* **2007**, *440*, 263−267.

(16) (a) Towatari, M.; Hamamatsu, T.; Yabe, K.; Matsumoto, N.; Mrozinski, J. Proceedings of XVth Winter School on Coordination Chemistry, Karpacz, Poland, Dec. 4−8, 2006. They reported complexes [Cu(3-MeOsaltn)(ac)Ln(hfac)$_2$] (Ln = Gd^{III}, Dy^{III}, Tb^{III}). (b) Towatari,

M.; Matsumoto, N.; Kojima, M.; Re, N.; Mrozinski, J. Proceedings of VIX th Annual Symmposium on Coordination Chemistry of Japan, 2PB-013 2009. Nagasaki, Japan. They reported the systematic syntheses and magnetic properties of binuclear M(II)−Ln(III) complexes.
(17) Ramade, I.; Kahn, O.; Jeannin, Y.; Robert, F. *Inorg. Chem.* **1997**, *36*, 930−936.
(18) (a) Fukuhara, C.; Tsuneyoshi, K.; Katsura, K.; Matsumoto, N.; Kida, S.; Mori, M. *Bull. Chem. Soc. Jpn.* **1989**, *62*, 3939−3943. (b) Fukuhara, C.; Tsuneyoshi, K.; Matsumoto, N.; Kida, S.; Mikuriya, M.; Mori, M. *J. Chem. Soc., Dalton Trans.* **1990**, 3473−3479.
(19) (a) Sakamoto, M.; Hashimura, M.; Matsuki, K.; Matsumoto, N.; Inoue, K.; Okawa, H. *Bull. Chem. Soc. Jpn.* **1991**, *64*, 3639−3641. (b) Costes, J. P.; Dahan, F.; Dupuis, A.; Laurent, J.-P. *Inorg. Chem.* **1996**, *35*, 2400−2402. (c) Miyasaka, H.; Matsumoto, N.; Okawa, H.; Re, N.; Gallo, E.; Floriani, C. *Angew. Chem., Int. Ed. Engl.* **1995**, *34*, 1446−1448.
(20) (a) Wang et al. reported Ni^{II}−Gd^{III} complex of $[Ni(3\text{-MeOsaltn})(MeOH)_2Ln(NO_3)_3]$. Wang, J.-H.; Yan, P. F.; Li, G. M.; Zhang, J. W.; Chen, P.; Suda, M.; Einaga, Y. *Inorg. Chim. Acta* **2010**, *363*, 3706−3713. (b) Andruh et al. reported a series of $[Ni(3\text{-MeOsaltn})Ln(NO_3)_3]$ and $[Zn(3\text{-MeOsaltn})Ln(NO_3)_3]$. Pasatoiu, T. D.; Tiseanu, C.; Madalan, A. M.; Jurca, B.; Duhayon, C.; Sutter, J. P.; Andruh, M. *Inorg. Chem.* **2011**, *50*, 5890−5898. (c) Pasatoiu, T. D.; Tiseanu, C.; Madalan, A. M.; Jurca, B.; Duhayon, C.; Sutter, J. P.; Andruh, M. *Inorg. Chem.* **2011**, *50*, 5879−5889.
(21) Casey, A. T.; Mitra, S. In *Theory and Applications of Molecular Paramagnetism*; Boudreaux, E.A., Mulay, L.N., Eds.; Interscience: New York, 1976; pp 135 and 271.
(22) Costes, J. P.; Dahan, F.; Dupuis, A.; Laurent, J. P. *Inorg. Chem.* **1997**, *36*, 4284−4286.
(23) Chen, Q. Y.; Luo, Q.; Zheng, L. M.; Wang, Z. L.; Chen, J. T. *Inorg. Chem.* **2002**, *41*, 605−609.
(24) Kahn, O. *Molecular Magnetism*; VCH: Weinhein, 1993; Part 6.4 and references therein.
(25) (a) Hudak, J.; Boca, R.; Dlhan, L.; Kozisek, J.; Moncol, J. *Polyhedron* **2011**, *30*, 1367−1373. (b) Titis, J.; Boca, R. *Inorg. Chem.* **2011**, *50*, 11838−11845.
(26) Costes, J. P.; Dahan, F.; Garcia-Tojal, J. *Chem.—Eur. J.* **2002**, *8*, 5430−5434.
(27) Kahn, M. L.; Mathoniere, C.; Kahn, O. *Inorg. Chem.* **1999**, *38*, 3692−3697.
(28) (a) Costes, J. P.; Dahan, F.; Dupuis, A.; Laurent, J.-P. *Chem.—Eur. J.* **1998**, *4*, 1616−1620. (b) Costes, J. P.; Donnadieu, B.; Gheorghe, R.; Novitchi, G.; Tuchagues, J. P.; Vendier, L. *Eur. J. Inorg. Chem.* **2008**, 5235−5244. (c) Kido, T.; Ikuta, Y.; Sunatsuki, Y.; Ogawa, Y.; Matsumoto, N.; Re, N. *Inorg. Chem.* **2003**, *42*, 398−408.
(29) Daiguebonne, C.; Guillou, O.; Kahn, M.; Kahn, O.; Oushoorn, R. L.; Boubekeur, K. *Inorg. Chem.* **2001**, *40*, 176−178.
(30) Shimada, T.; Okazawa, A.; Kojima, N.; Yoshii, S.; Nojiri, H.; Ishida, T. *Inorg. Chem.* **2011**, *50*, 10555−10557. (b) Ishida, T.; Watanabe, R.; Fujiwara, K.; Okazawa, A.; Kojima, N.; Tanaka, G.; Yoshii, S.; Noriji, H. *Dalton Trans.* **2012**, *41*, 13609−13619.
(31) Shiga, T.; Ohba, M.; Okawa, H. *Inorg. Chem.* **2004**, *43*, 4435−4446.
(32) (a) Castro, S. L.; Sun, Z.; Grant, C. M.; Bollinger, J. C.; Hendrickson, D. N.; Christou, G. *J. Am. Chem. Soc.* **1998**, *120*, 2365−2375. (b) Ako, A.; Mereacre, M.; Hewitt, I. J.; Clerac, R.; Lecren, L.; Anson, C. E.; Powell, A. K. *J. Mater. Chem.* **2006**, *16*, 2579−2586. (c) Okazawa, A.; Nojiri, H.; Ishida, T.; Kojima, N. *Polyhedron* **2011**, *30*, 3140−3144.
(33) Cole, K. S.; Cole, H. R. *J. Chem. Phys.* **1941**, *9*, 341−351.
(34) Sessoli, R.; Powell, A. K. *Coord. Chem. Rev.* **2009**, *253*, 2328−2341.
(35) (a) Gatteschi, D.; Sessoli, R.; Villain, J. *Molecular Nanomagnets*; Oxford University Press, New York, 2006. (b) Gatteschi, D.; Sessoli, R. *Angew. Chem., Int. Ed.* **2003**, *42*, 268−297.
(36) Colacio, E.; Ruiz-Sanchez, J.; White, F. J.; Brechin, E. K. *Inorg. Chem.* **2011**, *50*, 7268−7273.
(37) Gruber, S. J.; Harris, C. M.; Sinn, E. *J. Inorg. Nucl. Chem.* **1968**, *30*, 1805−1830.
(38) *Crystalstructure 3.7.0, Crystal Structure Analysis Package*; Rigaku and Rigaku/MSC: The Woodlands, TX, 2000−2005.